

LYMAN BREAK GALAXIES AT $Z \gtrsim 4$ AND THE EVOLUTION OF THE UV LUMINOSITY DENSITY AT HIGH REDSHIFT¹

CHARLES C. STEIDEL² AND KURT L. ADELBERGER
Palomar Observatory, Caltech 105–24, Pasadena, CA 91125

MAURO GIAVALISCO³
The Carnegie Observatories, 813 Santa Barbara Street, Pasadena, CA 91101

MARK DICKINSON^{4,5}
Department of Physics and Astronomy, The Johns Hopkins University, Baltimore, MD 21218

MAX PETTINI
Royal Greenwich Observatory, Madingley Road, Cambridge CB3 0EZ, UK

ABSTRACT

We present initial results of a survey for star-forming galaxies in the redshift range $3.8 \lesssim z \lesssim 4.5$. This sample consists of a photometric catalog of 244 galaxies culled from a total solid angle of 0.23 square degrees to an apparent magnitude of $I_{AB} = 25.0$. Spectroscopic redshifts in the range $3.61 \leq z \leq 4.81$ have been obtained for 48 of these galaxies; their median redshift is $\langle z \rangle = 4.13$. Selecting these galaxies in a manner entirely analogous to our large survey for Lyman break galaxies at smaller redshift ($2.7 \lesssim z \lesssim 3.4$) allows a relatively clean differential comparison between the populations and integrated luminosity density at these two cosmic epochs. Over the same range of UV luminosity, the spectroscopic properties of the galaxy samples at $z \sim 4$ and $z \sim 3$ are indistinguishable, as are the luminosity function shapes and the total integrated UV luminosity densities ($\rho_{UV}(z=3)/\rho_{UV}(z=4) = 1.1 \pm 0.3$). We see no evidence at these bright magnitudes for the steep decline in the star formation density inferred from fainter photometric Lyman-break galaxies in the Hubble Deep Field (HDF).

¹Based on data obtained at the Palomar Observatory, the Cerro–Tololo Inter-American Observatory, the William Herschel Telescope, and the W.M. Keck Observatory. The W. M. Keck Observatory is operated as a scientific partnership among the California Institute of Technology, the University of California, and NASA, and was made possible by the generous financial support of the W.M. Keck Foundation.

²NSF Young Investigator

³Hubble Fellow

⁴Allan C. Davis Fellow

⁵also Space Telescope Science Institute, 3700 San Martin Drive, Baltimore, MD 21218

The HDF provides the only existing data on Lyman-break galaxy number densities at fainter magnitudes. We have reanalyzed the $z \sim 3$ and $z \sim 4$ Lyman-break galaxies in the HDF using our improved knowledge of the spectral energy distributions of these galaxies, and we find, like previous authors, that faint Lyman-break galaxies appear to be significantly rarer at $z \sim 4$ than $z \sim 3$. This might signal a large change in the faint-end slope of the Lyman-break galaxy luminosity function between redshifts $z \sim 3$ and $z \sim 4$, but the $z \sim 4$ statistics are poor in the HDF, and we would expect (from our much larger ground-based surveys) a significant variance in Lyman-break galaxy number counts within the relatively small volumes probed by the HDF at high redshift. If the true luminosity density at $z \sim 4$ is somewhat higher than implied by the HDF, as our ground-based sample suggests, then the emissivity of star formation as a function of redshift would appear essentially constant for all $z > 1$ once internally consistent corrections for dust are made. This suggests that there may be no obvious peak in star formation activity, and that the onset of substantial star formation in galaxies might occur at $z \gtrsim 4.5$.

Subject headings: galaxies: evolution — galaxies: formation — galaxies: distances and redshifts — large scale structure of the universe

1. INTRODUCTION

Within the last few years it has become possible to undertake large surveys of galaxies at very large redshifts ($z > 2$). Simple photometric techniques keyed to the passage of the Lyman break through broad-band filters allow efficient selection of high redshift galaxy candidates (Steidel, Pettini & Hamilton 1995; Steidel *et al.* 1996a,b; Madau *et al.* 1996) which can then be confirmed and studied thanks to the large spectroscopic throughput of the Low Resolution Imaging Spectrograph on the W.M. Keck 10m telescopes (Oke *et al.* 1995). It is now feasible to study the large-scale distribution of star-forming galaxies at high redshift (Steidel *et al.* 1998; Giavalisco *et al.* 1998; Adelberger *et al.* 1998), and to obtain large enough samples of galaxies that accurate luminosity functions, color distributions, and the like for $z \sim 3$ objects can be compiled (e.g., Dickinson 1998; Steidel *et al.* 1998b). The advantage of large and reasonably well defined samples is that they allow direct comparisons to the predictions of galaxy and structure formation models (e.g., Baugh *et al.* 1998; Governato *et al.* 1998; Katz, Hernquist, & Weinberg 1998; Wechsler *et al.* 1998; Somerville, Primack, & Faber 1998; Coles *et al.* 1998; Bagla 1998; Jing & Suto 1998).

Most of the work up to the present has concentrated on the redshift regime $2.5 \lesssim z \lesssim 3.5$, for primarily practical reasons. These are the lowest redshifts at which the so-called “Lyman-break” technique can be applied using ground-based photometry. Also, at $z \sim 3$ the spectroscopic features that are most useful for determining the redshifts of Lyman-break galaxies (LBGs) fall within the wavelength range for which optical spectrographs are most efficient, and in which the

night sky background is minimal. As discussed by Steidel *et al.* 1998b, while conceptually it is straightforward to extend the Lyman-break technique to higher redshift (one simply uses a filter system that is shifted to longer wavelengths), the spectroscopic confirmation of photometrically selected objects becomes far more difficult.

The Lyman-break technique has already been used in a very powerful way in the Hubble Deep Field to estimate the star formation history of the Universe in coarse redshift bins defined by galaxies’ Lyman breaks passing through the F300W, F450W, and F606W filters (Madau *et al.* 1996; Madau, Pozzetti, & Dickinson 1998, hereafter MPD). It has now become a major industry to place any observation of high redshift objects in the context of their implied contribution to the history of star formation, using the Hubble Deep Field (HDF) observations as the basis for comparison at high redshifts ($z \gtrsim 2$). Possibly one of the most important results from a series of papers by Madau and others is the large apparent increase in ultraviolet luminosity density between redshift bins centered at $\langle z \rangle \approx 4$ and $\langle z \rangle \approx 2.75$, which suggests a rapid increase in the co-moving volume-averaged rate of star formation over a rather short interval of cosmic time. This intriguing result appears to be consistent with what is observed for the space density of luminous, high redshift QSOs (e.g. Schmidt *et al.* 1995, Kenefick *et al.* 1995, Shaver *et al.* 1998), and implies that at $z \gtrsim 4$ one is entering the “dark ages,” the epoch when star formation was first turning on in galaxies. Some other studies using photometric redshifts in the HDF, however, did not find evidence for such a clear change in the UV luminosity density over this redshift range (e.g. Sawicki *et al.* 1997; Pascarelle *et al.* 1999).

There are several reasons to be concerned about results based solely on the Hubble Deep Field, however. First, the HDF, while clearly the highest quality image of the sky ever obtained, is after all only a very small piece of sky, and samples a relatively small volume at any redshift. Since observations of the Lyman-break galaxies at $z \sim 3$ in ground-based surveys have shown that high redshift (luminous) star-forming galaxies are strongly clustered (Steidel *et al.* 1998a, Giavalisco *et al.* 1998, Adelberger *et al.* 1998), one might be concerned about sample variance associated with a relatively small volume. Moreover, even if the HDF provided a fair sample of the universe, the redshift distributions of F300W and F450W dropouts are not well known empirically. As a result, the effective volumes used by Madau *et al.* to calculate the star-formation densities at $\langle z \rangle = 2.75$ and $\langle z \rangle = 4$ were based upon models of the spectral-energy distributions and Lyman-continuum opacities of galaxies, and not on spectroscopic redshifts. We have found, in our large survey at $z \sim 3$, that the effective redshift selection function imposed by a particular set of photometric selection criteria is not a simple “boxcar” as assumed by Madau *et al.* Objects near the assumed boundaries of the $N(z)$ function are under-represented due to photometric errors, and, more importantly, to the fact that there are substantial variations in the spectra of galaxies at a given redshift. These variations are due, among other things, to the stochastic nature of the line blanketing in the Lyman α forest, to the amount of intrinsic reddening by dust, and to whether Lyman α is in emission or absorption. While such subtleties may not seem important for the rather crude luminosity densities estimated from photometric redshifts, they undoubtedly

have at least some effect on the implied luminosity densities, and the magnitude of this effect is difficult to estimate without spectroscopic redshifts.

In view of the importance of confirming the decline in the far-UV luminosity density between $z \sim 3$ and $z \sim 4$, and the fact that we now have a substantial sample of galaxies in the redshift range $2.6 \lesssim z \lesssim 3.4$ from our relatively wide-angle ground-based surveys, we have undertaken to compile wide-field photometry and spectroscopic confirmation of Lyman-break galaxies in a redshift interval $3.8 \lesssim z \lesssim 4.5$.

Although comparatively low spatial resolution and significantly brighter backgrounds make it difficult to reach the depth of the HDF from the ground, it is feasible to survey much larger fields; our present survey aims to exploit this advantage. We have attempted to reach depths for $z \sim 4$ LBGs that are comparable to our existing survey at $z \sim 3$, over a region ~ 160 times larger than the HDF. The $z \sim 3$ survey has been based entirely on the custom U_nGR filter system (described in detail in Steidel & Hamilton 1993), with effective wavelengths of 3650, 4870, and 6930 Å, respectively. It turns out to be remarkably efficient, for the purposes of selecting Lyman-break galaxies at $z \gtrsim 4$, to add one passband (I , with an effective wavelength of 8100 Å) to our existing imaging data, and to select G -band dropouts using the GRI system in a manner entirely analogous to the way we have used U_nGR at $z \sim 3$.

In this paper, we present the initial results of our galaxy survey with an expected median redshift of $\langle z \rangle = 4.2$, to demonstrate the feasibility of extending spectroscopic Lyman-break galaxy surveys to higher redshifts, and to make a preliminary estimate of the star formation luminosity density for comparison to the analogous value at $z \sim 3$, all based on data that are independent of the Hubble Deep Field.

2. PHOTOMETRIC SELECTION CRITERIA

The photometric selection criteria, as for our $z \sim 3$ sample, are based upon a combination of the expectations from modeling the spectral energy distributions of star-forming objects at high redshift, combined with practical considerations such as allowing for photometric errors, and steering away from regions in the GRI color–color plane that are obviously contaminated with objects that are *not* at very high redshift (i.e., “interlopers”). Our intention initially was to err on the side of caution and obtain redshifts for objects with a rather broad range of colors, since we did not know *a priori* where in the GRI color–color plane the population of $z \sim 4$ objects would lie.

We defined the initial color selection criteria with the observed range of intrinsic $z \sim 3$ galaxy colors in mind. As will be discussed elsewhere (Adelberger *et al.* 1999), the colors of the galaxies in our $z \sim 3$ sample are consistent with standard Bruzual and Charlot (1996) models of continuous star formation, altered by the statistical opacity of the IGM (following Madau 1995) and a

component of optically thick H I in the galaxy itself⁶, and reddened by applying a version of the starburst galaxy obscuration relation of Calzetti (1997) extrapolated to wavelengths shorter than 1200 Å. The range of UV colors observed in the $z \sim 3$ sample is well represented by such models with $E(B - V)$ ranging from zero to ~ 0.3 magnitudes, with a median color (which can be thought of as the spectrum of the “typical” Lyman-break galaxy in the $z \sim 3$ sample) corresponding to $E(B - V) = 0.15$ for the adopted reddening curve (note that this corresponds to an extinction at rest-frame ~ 1700 Å [the observed \mathcal{R} band] of about a factor of 4). All magnitudes and colors used in this paper are reported on the “AB” system (Oke & Gunn 1983).

Our GRI photometric selection criteria were designed to select galaxies at $z \sim 4$ with a range of intrinsic SEDs similar to what is observed in our U_nGR sample at $z \sim 3$. In Figure 1a, we have plotted the tracks in the GRI color–color plane for the model spectra which closely match the observed galaxies at $z \sim 3$; the same model galaxies are plotted in Figure 1b to show their location relative to the color selection window used for the $z \sim 3$ sample. There are two different color selection windows indicated in Figure 1a. The shaded region is the one actually used to select objects for spectroscopic follow-up, which was intended to be relatively broad in order to explore the color–color space (and the effects of photometric scatter) somewhat; the bold line encompasses the region which we will use as our primary selection window for comparison with the $z \sim 3$ data. The latter was adopted because it would result in comparable effective volumes near $\langle z \rangle = 4.2$ and $\langle z \rangle = 3.05$ in our two surveys if galaxies had the same range of intrinsic colors at these redshifts, and also because (as we shall see below) it turns out that one can eliminate a substantial fraction of the interlopers by keeping the $\mathcal{R} - I$ colors relatively blue. This selection window is defined by

$$G - \mathcal{R} \geq 2.0, \quad G - \mathcal{R} \geq 2(\mathcal{R} - I) + 1.5, \quad \mathcal{R} - I \leq 0.6.$$

The “median color” galaxy model (the middle of the three color-color tracks shown in Figure 1a) enters the primary selection window at $z \sim 3.9$, and exits again at $z \sim 4.5$, so that this would be the *a priori* expected redshift range of a galaxy sample similar to the one observed at $z \sim 3$. This figure also shows that bluer (i.e., less reddened) galaxies are expected to be biased somewhat toward the higher redshifts, and redder (i.e., more reddened) ones toward the lower redshifts; this is the main effect that makes the realized $N(z)$ function different from a “boxcar” (see, e.g., Steidel *et al.* 1998b, and Figure 4). In Figure 1a we have also plotted the color tracks for a template elliptical galaxy, with only k-corrections applied (i.e., no spectral evolution). Note that the locus of unevolved early type galaxies comes very close to the selection window for the $z \sim 4$ galaxies for $z \sim 0.5 - 1$. A combination of photometric errors and intrinsic variations in galaxy spectral-energy distributions can scatter some early-type galaxies at these redshifts into our selection window. It turns out that such objects are the sole source of “interlopers” for the $z \gtrsim 4$ sample, and we suggest below ways that their contribution can be minimized. Note also that no contamination by stars is expected (unlike in the $z \sim 3$ sample—see Figure 1b).

⁶This component has not generally been included in past work

3. OBSERVATIONS

3.1. Imaging

With the exception of DSF1550, all of the fields included here have been part of our extensive survey for $z \sim 3$ galaxies; the field centers are given in Table 1. The imaging data were obtained at the William Herschel telescope (3C 324 and B2 0902+34), Palomar 200-inch Hale telescope (CDFa, CDFb, DSF2237a, DSF2237b, SSA22a, SSA22b, and B2 0902+34), and the CTIO 4m telescope (DSF1550+08) during the interval 1996-98. All of the imaging data and the photometric methods employed will be presented in detail elsewhere; in brief, the photometry was performed in a manner identical to that used for the $z \sim 3$ galaxy searches, which is described (for example) in Steidel, Pettini, & Hamilton (1995), with the exception that we have used a modified version of the FOCAS (Valdes 1982) image detection and analysis routines that one of us (KLA) has optimized for our purposes.

For fields in which existing U_nGR catalogs were already on hand, we simply registered the I image onto the same coordinate system and obtained the I magnitudes and $\mathcal{R} - I$ colors through the same matched apertures. We have performed our object detection on the \mathcal{R} band images because they are in most cases significantly deeper than in the I band. However, the selection of candidate $z \sim 4$ galaxies has been made using the I band total magnitudes. (This procedure is unlikely to present any significant biases, given that the expected colors are quite blue in $\mathcal{R} - I$, and our \mathcal{R} images typically reach ~ 0.5 magnitudes deeper than the I images). The typical depths of our images, in $\sim 1''$ seeing, are 29.3, 28.5, and 28.0 magnitudes per square arc second for G , \mathcal{R} , and I , respectively, within a $1''$ aperture (1σ). Thus, an object with $I = 25$ is approximately a $5 - 10\sigma$ detection in the I band, with considerable dynamic range available to measure colors in the G and \mathcal{R} bands.

We have chosen to limit the object catalogs to $I \leq 25.0$ in order to provide a relatively high level of photometric completeness and ensure that there would be sufficient dynamic range to detect breaks in the $G - \mathcal{R}$ colors. We will discuss completeness issues in §4 below.

The photometric selection criteria summarized in Figure 1a (shaded region) were used to isolate candidates for $z \gtrsim 4$ objects. All such candidates were examined visually in order to remove objects that were clearly spurious (these usually were found near very bright stars). A summary of the number of remaining candidates in each field is given in Table 1. A composite 2-color diagram from the 10 fields included in this paper is shown in Figure 2.

3.2. Spectroscopy

All of the galaxy spectra were obtained using the Low Resolution Imaging Spectrograph (Oke *et al.* 1995) on the Keck II 10m telescope, between 1997 March and 1998 October. For the observing runs in 1997, we generally included several slits targeting $z \sim 4$ candidates on

masks designed primarily for our $z \sim 3$ LBG survey; as a consequence, most of these spectra were obtained using the 300 line/mm grating blazed at 5000 Å and with a grating tilt optimized for the 4000–7000 Å range. A more efficient configuration, with better sensitivity in the crucial 6000–7500 Å range, was to use a 150 line/mm grating blazed at 7500Å; this was used in the 1998 observing runs and increased the spectroscopic success rate by about a factor of 2–3 for both $z \sim 4$ galaxies and lower redshift interlopers (e.g., a single slit mask, with 16 candidate objects, yielded 7 successful redshifts in the $3.9 \leq z \leq 4.5$ and one $z = 0.96$ interloper in the DSF1550 field in 1998 May—the remaining 8 candidates had inadequate S/N for identification). Slit widths on the masks were either 1"0 or 1"4, resulting in spectral resolution ranging from 10–12Å for the 300 line configuration and 20–25Å for the 150 line configuration. Typical total exposure times per mask were 2 hours, usually broken into individual exposures of 1200 or 1800s, with small dithers along the slitlets between exposures in order to sample different parts of the detector and to allow the option of various schemes for the removal of fringes at redder wavelengths. The data were reduced using a suite of custom IRAF scripts.

Examples of $z \sim 4$ galaxy spectra are shown in Figure 3. The onset of strong Lyman α forest blanketing is very apparent in the spectra of these galaxies. As in the $z \sim 3$ sample, there is a wide variety of spectroscopic properties, ranging from Lyman α in emission with rest-frame equivalent widths up to ~ 80 Å, to objects with very strong Lyman α absorption and accompanying strong lines of various interstellar transitions of low ions, to objects that have Lyman α in both absorption and in emission (see, e.g., the spectrum of HDF G4 in Figure 3). There is an obvious spectroscopic bias against objects that do not have strong emission lines, but even with this bias about half of our successful redshifts are based purely on absorption features. The substantial fraction of absorption-dominated spectra in our $z \sim 4$ sample may be due in part to the large intrinsic luminosities of the galaxies; we see some evidence in our $z \sim 3$ sample, which reaches fainter intrinsic luminosities, that brighter objects tend to have absorption-dominated spectra. These effects will be quantified elsewhere.

Unsuccessful redshifts were invariably due to lack of adequate S/N. This is a more serious problem at $z \sim 4$ than at $z \sim 3$, largely because the spectral features used to identify redshifts are moved from 4500–6000 Å to 6500–7500 Å, where the sky is 1.5–2 magnitudes brighter. As a result our success rate for identifying redshifts is ~ 30 –50% at $z \sim 4$, compared to $\gtrsim 80\%$ at $z \sim 3$. Objects with strong Lyman α emission lines are clearly less likely to fall into the “unsuccessful” category, as the continuum S/N is much less important than for the absorption line objects, and for this reason it is likely that most of the spectra which remain to be identified do not have Lyman α emission with large equivalent width. In the range of continuum luminosity that we are currently probing, even very sensitive narrow-band searches would turn up only a relatively small fraction of the galaxies (cf. Hu *et al.* 1998).

The magnitudes, colors, and redshifts of all 48 of the spectroscopically confirmed $z \gtrsim 4$ galaxies are summarized in Table 2. Also summarized are the same quantities for the galaxies identified as interlopers; all 73 of the objects with redshifts are indicated with shaded “dots” on

Figure 2. From Figure 2, it is clear that most of the objects in the selection window with red $\mathcal{R} - I$ colors are interlopers. As mentioned above, by tightening the color selection window to include only objects having $\mathcal{R} - I \leq 0.6$, one immediately eliminates 11 of the 25 interlopers, most of which have $z \sim 1$, as expected from Figure 1a; only 2 out of 48 of the bona fide high redshift galaxies are excluded⁷. In addition, applying the requirement that the galaxies must have $I \geq 23.0$ (this will tend to screen out $z \sim 0.5$ early type galaxies, which will typically have $I \sim 21 - 22$) eliminates an additional 2 interlopers in the spectroscopic sample, and has no effect on the true high redshift sample for objects with redshifts. Thus, with this adjustment of the color selection criteria (which one would have chosen in any case in order to observe the same types of galaxies seen in the $z \sim 3$ sample, as demonstrated in Figure 1), the contamination of the spectroscopic sample can be reduced from 25/73 to 12/60, with the loss of only 2 true high redshift galaxies. As can be seen from Table 1, applying the new color cut reduces the number of candidates from 244 to 207. We regard this sample of 207 candidates as our primary photometric sample⁸, and the estimated contamination by interlopers is $\sim 20\%$.

4. DIFFERENTIAL COMPARISONS: $z \sim 4$ VERSUS $z \sim 3$

4.1. Correcting for Incompleteness

The observed surface density of $z \sim 4$ galaxies to a limit of $I = 25.0$, $\Sigma_4(25) = 0.20 \pm 0.02$ arcmin⁻², is significantly smaller than the observed surface density of $z \sim 3$ galaxies to $\mathcal{R} = 25.0$, $\Sigma_3(25) = 0.68 \pm 0.03$ arcmin⁻². The I band samples the far-UV continuum of $z \sim 4$ galaxies at very similar rest wavelengths as the \mathcal{R} band at $z \sim 3$ (by design), so that k-corrections between the two should be negligible; however, obviously one is sampling different parts of the luminosity function because of the larger luminosity distance for the $z \sim 4$ sample. Our approach for comparing the two samples will be to truncate the $z \sim 3$ sample at an apparent \mathcal{R} magnitude that corresponds to an absolute far-UV flux density equivalent to $I = 25.0$ at $z = 4.13$ (the median redshift of the $z \sim 4$ sample). This apparent magnitude is cosmology dependent: $\mathcal{R} = 24.51$ for Einstein-de Sitter, $\mathcal{R} = 24.31$ for $\Omega_0 = 0.2$ open, and $\mathcal{R} = 24.45$ for $\Omega_0 = 0.3$, $\Omega_\Lambda = 0.7$.

The first step is to correct the samples for contamination by interlopers. The $z \sim 4$ surface density was statistically corrected for contamination based on the spectroscopic results, as described above. At $z \sim 3$, the only known interlopers (other than QSOs, which we have also removed from the sample) are Galactic stars, which we have found empirically to have a surface

⁷One of these, CDFa-G1 at $z = 4.812$, is the most intrinsically luminous Lyman break galaxy in our entire sample of more than 700 at $z > 2$. The relatively red $\mathcal{R} - I$ color in this case is due to significant blanketing of the \mathcal{R} passband by the Lyman alpha forest.

⁸ The effect on the net surface density of candidates after correction for interlopers is barely affected by this cut; the contamination-corrected number of candidates is $244(48/73) = 160$ without the cut, and $207(46/58) = 164$, or a difference of much less than 1σ

density to $\mathcal{R} = 24.0$ along the sightlines we sample of $\Sigma_{\text{stars}} = 0.06 \text{ arc min}^{-2}$ (and essentially zero at fainter apparent magnitudes). Thus, both samples have comparable contamination by interlopers, and both interloper populations (stars and early type galaxies) tend to populate the bright end of the apparent magnitude distribution; all corrections for contamination have been made as a function of apparent magnitude.

Once interlopers have been removed from the samples, we can begin to estimate the comoving luminosity density at $z \sim 3$ and $z \sim 4$ from the observed surface density of U_n and G dropouts. The main complication is that some fraction of the galaxies brighter than our magnitude limits at these redshifts are undoubtedly missing from our sample because of photometric errors, blending with foreground objects, and—more seriously—because they may have intrinsic colors which do not match our selection criteria. In order to investigate this incompleteness quantitatively, we have run Monte-Carlo simulations in which large numbers of artificial objects with a range of colors and magnitudes are added to our real images, and then recovered using the same methods employed for the real photometry. The complete results of these simulations will be presented in Adelberger *et al.* (1999, A99); but for the present they are useful mainly because they yield an estimate of the effective volume of our surveys as a function of apparent magnitude,

$$V_{\text{eff}}(m) \equiv \int dz p(m, z) dV/dz,$$

where $p(m, z)$ is the probability a galaxy of apparent magnitude m (in \mathcal{R} at $z \sim 3$ and I at $z \sim 4$) at redshift z will be detected in our images and appear to match our photometric criteria, and $dz dV/dz$ is the comoving volume per arcmin² at redshift z . As shown in A99, dividing the observed surface density of high redshift candidates by $V_{\text{eff}}(m)$ defined in this way compensates for our various selection biases and incompletenesses, and produces a maximum likelihood estimate of the comoving number density of galaxies with magnitude m at the observed redshifts. The galaxy number density estimated with this procedure is corrected not only for the usual “detection incompleteness” due to the declining probability of detecting a galaxy in our images at the faintest magnitudes (caused by both photometric errors and problems related to blending with foreground objects⁹), but also for “color incompleteness” due to detected galaxies having measured colors that may erroneously place them outside of our color-selection window, and even to some extent for the “template incompleteness” which would arise if some fraction of high-redshift galaxies had true colors that lay outside of our color-selection window. This last correction is possible because our U_nGR sample (for example) could contain galaxies at $z \sim 2.5$ much redder than the typical color we assume, and galaxies at $z \sim 3.5$ much bluer, and we can therefore use data from these redshifts to estimate the fraction of galaxies whose colors will not match our selection criteria at $z \simeq 3$, where most of our sample lies. We will return to this below.

The effective volumes calculated from our Monte-Carlo simulations are provided, as a function of apparent magnitude, in Tables 3 and 4. The incompleteness corrections implied by these

⁹The completeness correction for even the brightest magnitude bin is $\sim 30\%$, due mostly to blending effects.

effective volumes are significant, but because the corrections are comparable (to within $\sim 30\%$) for the $z \sim 3$ and $z \sim 4$ samples, they do not strongly affect our estimate of the change in luminosity density over this range of redshift. Very similar relative volumes at $z \sim 3$ and $z \sim 4$ would result, for example, from simply assuming a boxcar selection function with half-width given by the standard deviation (see Figure 4) of the redshifts in each sample. The incompleteness corrections are important when we attempt to derive absolute UV luminosity densities at $z \sim 3$ and $z \sim 4$, but this calculation is subject to other, probably larger, uncertainties, as we discuss below.

4.2. Color and Luminosity Distributions

From these effective volumes it is straightforward to compute luminosity functions from the observed surface density of U_n and G dropouts. It is of primary interest to compare the luminosity functions, and the integral luminosity densities, in the two redshift intervals. The most recent compilation from the Hubble Deep Field data is that of Madau, Pozzetti, & Dickinson (1998, MPD), which suggests a factor of ~ 2.5 decline in the luminosity density between $z \sim 2.75$ and $z \sim 4$ (the original Madau *et al.* 1996 paper estimated the same decline at a factor of ~ 4). In contrast we see little evidence in our ground-based sample for luminosity density evolution from $z \sim 4$ to $z \sim 3$. Figure 5 compares the U_n - and G -dropout luminosity functions for an Einstein-de Sitter cosmology. The agreement in both the shape and normalization of the bright end of the luminosity functions at $z \sim 3$ and $z \sim 4$ is quite striking, and depends only mildly on cosmology (the other 2 cosmologies considered make the $z \sim 4$ luminosity function slightly brighter relative to that at $z \sim 3$). To construct this plot from the comoving number density of objects with apparent magnitude m_{AB} , which we estimated above, we used the relationship $L_\nu = 10^{-0.4(48.60+m_{AB})}4\pi d_L^2/(1+z)$ and adopted (for simplicity) $\Omega_m = 1$ luminosity distances of $d_L = 3.8 \times 10^{28}h^{-1}$ cm for all objects in our $z \sim 3$ sample, and $d_L = 5.3 \times 10^{28}h^{-1}$ cm for all objects in our $z \sim 4$ sample. These luminosity distances are appropriate for objects at the median observed redshifts of $\langle z \rangle = 3.04$ and $\langle z \rangle = 4.13$. The corresponding luminosity distances for $\Omega_m = 0.2$ open and $\Omega_m = 0.3$ flat are $d_L = 5.8, 5.6 \times 10^{28}h^{-1}$ cm at $\langle z \rangle = 3.04$ and $d_L = 9.0, 8.1 \times 10^{28}h^{-1}$ cm at $\langle z \rangle = 4.13$.

The results of integrating the luminosity distributions over the same range of intrinsic luminosity (the smallest luminosity corresponds to the faintest objects in the $z \sim 4$ sample, which is $I = 25.0$, or $M_{AB}(1700\text{\AA}) = -21$ for the Einstein-de Sitter model $H_0 = 50 \text{ km s}^{-1}\text{Mpc}^{-1}$ [see Figure 5]), as well as the ratios of the luminosity densities in the two redshift intervals, are given in Table 5. In assigning errors to these luminosity densities, we have attempted to account for Poisson counting statistics, uncertainties in the contamination corrections, and for systematic uncertainties in the effective volumes discussed above.

For all cosmologies we consider, the observed UV-luminosity density integrated to the luminosity equivalent of $I_{AB} = 25.0$ at $z = 4.13$ shows no significant change between $\langle z \rangle = 4.13$ and $\langle z \rangle = 3.04$, in apparent conflict with several analyses based upon the HDF alone (e.g. Madau

et al. (1996), MPD, Pozzetti *et al.* 1998). We will return to this shortly.

A useful by-product of the estimated $V_{\text{eff}}(m)$ from A99 is the incompleteness-corrected distribution of intrinsic galaxy spectral shapes in our $z \sim 3$ sample, shown in Fig. 6 (see A99 for details of how this plot was constructed). For convenience we have chosen to parameterize the range of LBG spectral shapes by assuming that they arise due to varying amounts of reddening by dust imposed on otherwise identical model galaxies (see §2). This is obviously not an exact description of the physical situation, as (for example) the galaxies with negative $E(B - V)$ in Fig. 6 show¹⁰, and in fact some of the range of observed $G - \mathcal{R}$ colors at $z \sim 3$ can be traced to fluctuations in the strength of Lyman α emission or absorption, and some is undoubtedly due to fluctuations in intergalactic absorption and in star-formation histories among the galaxies in our sample. Nevertheless variable dust absorption is plausibly the dominant factor (cf. Pettini *et al.* 1998a, Dickinson 1998), and for this reason we have chosen to quantify deviations from the mean observed colors with $E(B - V)$. For our present purposes the physical cause of the spread in measured colors is irrelevant, however, and all that matters is that the family of spectral shapes implicit in this parameterization can reasonably approximate the entire range of far-UV spectral shapes in our $z \sim 3$ sample.

An interesting aspect of Figure 6 is the clear dearth of objects with $E(B - V) \gtrsim 0.3$. Our sample is slightly biased against reddened objects, but even after correcting for these selection effects the comoving number density of galaxies with $E(B - V) \sim 0.1$ is more than ten times higher than that of galaxies with $E(B - V) \sim 0.4$. We see no galaxies with $E(B - V) > 0.5$, though these galaxies—if they existed—would match our color criteria over the redshift range $2.5 \lesssim z \lesssim 2.7$.¹¹ Overall the histogram of $E(B - V)$ suggests that few galaxies at $z \sim 3$ are so red (or so blue) that they would be completely absent in our U_nGR sample.

4.3. The Hubble Deep Field

With this distribution of $E(B - V)$ in hand, it is possible to predict the redshift distributions of high-redshift color-selected samples with some accuracy. Figure 4 shows a comparison of the

¹⁰ In almost all cases, galaxies with negative values of $E(B-V)$ actually have continuum shapes consistent with $E(B-V)=0$, but they have unusually strong Lyman α emission (observed equivalent widths up to 300 Å), which can affect the measured $G - \mathcal{R}$ color by a few tenths of a magnitude at the extreme, until $z \sim 3.35$, at which point the Lyman α line moves out of the G band. For the present purposes, the incidence of such negative values of $E(B-V)$ simply indicates the relative numbers of such strong emission line galaxies. In the future, all galaxy colors will be corrected for Lyman α contamination. In general, however, the effect is small.

¹¹ Although a galaxy with $E(B - V) \sim 0.5$ would have the right colors to be included in our sample at $2.5 \lesssim z \lesssim 2.7$, the implied extinction (assuming the reddening were due to dust with the Calzetti (1997) reddening curve) would be 5.2 magnitudes, and these galaxies might be missing from our sample simply because they are too faint. However, we see no evidence in our sample that redder galaxies are systematically fainter. For example, the mean \mathcal{R} magnitude of the 4 galaxies in our sample with $0.4 < E(B - V) < 0.5$ is 24.6, somewhat brighter than average.

observed redshift distributions in our U_nGR and GRI samples with the redshift distributions that would be expected, given the adopted color selection criteria, if spectral shapes were drawn randomly from this histogram and the luminosity function were constant within each redshift interval. The agreement between the model predictions and the data, for both the color distribution as a function of redshift, and the overall redshift distribution, is reasonably good. This raises the hope that we might be able to get improved estimates of the apparently discrepant luminosity densities implied by F300W and F450W dropouts in the Hubble Deep Field if we used our distribution of $E(B - V)$ to estimate the effective volumes for the HDF color-selection criteria. Figure 7 shows the redshift distributions we would predict from our $E(B - V)$ distribution for galaxies selected according to the criteria

$$U_{300} - B_{450} \geq B_{450} - V_{606} + 1, \quad U_{300} - B_{450} \geq 1.6, \quad B_{450} - V_{606} \leq 1.2, \quad V_{606} \leq 27$$

and

$$B_{450} - V_{606} > 1.5, \quad B_{450} - V_{606} > 1.7(V_{606} - I_{814}) + 0.7$$

$$B_{450} - V_{606} < 3.5(V_{606} - I_{814}) + 1.5, \quad V_{606} - I_{814} < 1.5, \quad V_{606} < 27.7$$

for the U_{300} and B_{450} dropouts, respectively (cf. Dickinson (1998), Madau *et al.* (1996)). It has been assumed by Madau *et al.* (1996), MPD, Dickinson 1998, and Pozzetti *et al.* 1998 that these two selection criteria uniformly probe the redshift intervals $2.0 < z < 3.5$ and $3.5 < z < 4.5$. Our estimated redshift distributions are broadly in agreement with this, although the effective volumes we find, 380 (200) h^{-3} comoving $\text{Mpc}^3 \text{ arcmin}^{-2}$ for $\Omega = 1$, are 13% (19%) smaller at $z \sim 3$ (4). Unlike our effective volumes for the ground-based samples, these effective volumes do not include photometric errors; they account only for what we have called “template incompleteness” above—i.e., for the fraction of galaxies that would meet the HDF color-selection criteria in the absence of photometric errors, if all galaxies had intrinsic spectral shapes drawn from the distribution of A99 (see Figure 6 and the related discussion).

Figure 8 shows our estimate of the faint end of the luminosity functions at $z \sim 3$ and $z \sim 4$ derived from these effective volumes and the observed surface density of U_{300} and B_{450} dropouts in the HDF. For the U_{300} sample we used the approximation $\mathcal{R} \simeq (V_{606} + I_{814})/2$ and shifted all magnitudes 0.25 fainter to account for its smaller mean redshift ($\langle z \rangle \sim 2.6$) compared to our U_nGR sample. The number of U_{300} dropouts in the HDF was taken from the catalog of Dickinson (1998); the B_{450} dropouts are from table 3 of Madau *et al.* (1996).

The U_{300} dropout points fall rather nicely along the Schechter (1976) function with faint-end slope $\alpha \sim -1.6$ defined by the ground-based sample alone, but this is likely at least partly fortuitous: removing the $U_{300} - B_{450} > 1.6$ criterion from our U_{300} dropout definition would have changed our estimated effective volume by only 14%, but would have increased the number of U_{300} dropouts by about 45% and significantly altered the luminosity function shape. The large number of dropouts excluded by the $U_{300} - B_{450} > 1.6$ criterion have colors similar to those expected for galaxies at $z \simeq 2$, suggesting that a significant fraction of the U_{300} dropouts in the HDF may be associated with a single galaxy over-density at $z \sim 2$. This would not be completely unexpected;

even in one of our much larger ground-based fields, “SSA22a,” almost half of the U_n dropouts lie within the narrow redshift interval $3.07 < z < 3.11$ (Steidel *et al.* 1998a). Regardless of the exact cause of these changes, it appears that seemingly minor adjustments to color-selection criteria in the HDF can have serious effects on the normalization and shape of derived luminosity functions, and this illustrates that caution is required in interpreting the results from a single small field as universal. Measuring consistent luminosity functions in several fields spread over the sky would provide some assurance that the derived luminosity densities may be close to their universal values, but currently this is possible only at the relatively shallow depths reached in ground-based samples.

Nevertheless, we have fit a Schechter (1976) function to the combined HDF + ground-based luminosity function shown in Figure 8, after excluding the faintest HDF point which may suffer from incompleteness, and we find, with formal 68.3% confidence, that $m_* = 24.48 \pm 0.15$ and $\alpha = -1.60 \pm 0.13$. The fit is determined largely by the ground-based data, and so our confidence in it is not entirely eroded by our reservations about the HDF. This estimate of the faint-end slope α is considerably steeper than previous estimates (e.g. Dickinson 1998, Pozzetti *et al.* 1998)¹².

At $z \sim 4$ it is more difficult to gauge the consistency between the ground-based data and the HDF, because there is very little luminosity overlap between the two samples; only a single B_{450} dropout in the HDF would have been bright enough to be included in our ground-based sample. A naive fit to the points in the bottom panel of Figure 8 would favor a faint-end slope of $\alpha \sim -1$, but because of our concerns about sample variance in the HDF, we have chosen to plot (instead of an actual fit) our $z \sim 3$ luminosity function redshifted to $z \sim 4$ in an $\Omega = 1$ cosmology (i.e., with m^* shifted by the relative distance modulus between $z = 3.04$ and $z = 4.13$), and multiplied by 0.8 (cf. Table 5). This matches our $z \sim 4$ data well at the bright end, but over-predicts the number of fainter HDF B_{450} -dropouts by about a factor of two, and the integrated luminosity density by about a factor of 2.5 (see the discussion in §5.1). A combination of deeper ground-based data and the HDF-South should help decide whether the disagreement of the HDF B_{450} dropouts at the faint end truly signals a different luminosity function shape at $z \sim 4$, or is a further indication that the HDF does not provide a fair sample of the universe.

4.4. The Evolution of the UV Luminosity Density

Figure 8 contains most of the available information on the star-formation density at $z \sim 3$ and $z \sim 4$, and we have used it as a basis for re-evaluating the star-formation history of the universe derived previously by many authors, most famously Madau *et al.* (1996). Our result is shown in the top panel of Figure 9. For consistency we estimated the star-formation density of the universe

¹²The difference between the new luminosity function and that presented by Dickinson (1998) is due to slightly modified selection criteria in the HDF and (especially) to improved estimates of incompleteness in the ground-based sample.

at all redshifts by integrating luminosity functions down to $0.1L^*$, which corresponds roughly to $\mathcal{R} = 27$, our faintest data point, at $z \sim 3$. As discussed above, the luminosity functions at $z \sim 3$ and (especially) $z \sim 4$ have not been convincingly measured down to $0.1L^*$, and this is one of the many large uncertainties that underlie a diagram such as Figure 9. At $z \sim 3$ we adopted the $m_* = 24.48$, $\alpha = -1.60$ Schechter-function fit derived above for the luminosity function. At $z \sim 4$ we used the luminosity function form shown in the bottom panel of Figure 8; as discussed above, this luminosity function agrees well with the $z \sim 4$ data at the bright end, but is apparently inconsistent at the faint end with the small number (13) of B_{450} dropouts in the HDF. The estimate of the star-formation density at $z \sim 1$ relies upon luminosity functions at lower redshifts in a similar way: because the high-redshift CFRS data do not extend past L^* , the faint-end slope from lower redshift points was assumed in calculating the integral luminosity density at $z \sim 1$. The ground-based point at $z \sim 3$ is in very good agreement with that from MPD based solely on the HDF, because the new effective volume is similar to that assumed in the past, but we find no evidence for a sharp decline at any redshift larger than $z \sim 1$. If we were to integrate the luminosity functions over all luminosities instead of over $L > 0.1L^*$, the total luminosity density for our $z \sim 3$ and $z \sim 4$ points would be increased by an additional factor of $1.7_{-0.2}^{+0.6}$, whereas the $z \lesssim 1$ points would increase by only $\sim 20\%$. This is due to the different faint-end slopes ($\alpha = -1.60$ and $\alpha = -1.3$) that we have assumed at $z \gtrsim 3$ and $z \lesssim 1$. It is clear that the real uncertainties in the absolute placement of any of the points in Figure 9 are much larger than the error bars would indicate when uncertainty in the shape of the luminosity function at unobserved magnitudes is taken into account.

The star-formation densities we have calculated so far assume that the far-UV continua of Lyman-break galaxies have not been extinguished by dust, but of course the observed colors of these galaxies suggest that this is unlikely to be the case. In principle we could correct each galaxy’s magnitude for dust extinction based upon its implied $E(B - V)$, construct new luminosity functions at $z \sim 3$ and $z \sim 4$, and then integrate these to obtain dust-corrected star formation densities. Unfortunately it is difficult to estimate $E(B - V)$ for galaxies in our $z \sim 4$ sample, because the \mathcal{R} and I filters do not provide a long enough wavelength baseline, and in any case the $z \sim 4$ spectroscopic sample is still rather small. For simplicity we have instead corrected our $z \sim 3$ and $z \sim 4$ star-formation densities for extinction by multiplying each by a factor of 4.7, appropriate for the Calzetti (1997) reddening law with typical $E(B - V) = 0.15$ (cf. Figure 6). This correction is reasonably well justified for the $z \sim 3$ sample, where we know the distribution of $E(B - V)$. Its justification at $z \sim 4$ depends upon the assumptions that dust properties are the same at $z \sim 3$ and $z \sim 4$ and that galaxies have the same underlying SEDs; these assumptions are at least consistent with the limited data, as (for example) Figure 4 shows. The extinction-corrected luminosity densities are shown in the bottom panel of Figure 9. In this figure we have also applied reddening corrections to the points at other redshifts. For internal consistency we assumed the same mean $E(B - V) \simeq 0.15$ and Calzetti extinction law for galaxies in other samples, so that differences in extinction corrections depend only on the different rest wavelengths probed at different redshifts. Under these assumption, the ratio of extinction corrections at $z > 2$ and

$z < 2$ is set by the ratio of the effective extinction at $\sim 1500\text{\AA}$ to that at 2800\AA , or a factor of approximately 1.7, implying a multiplicative correction to the $z < 2$ points of 2.7. The implied correction at $z \sim 1$ is consistent with the corrections deduced by Glazebrook *et al.* (1998) from $\text{H}\alpha$ spectroscopy of galaxies from the Canada-France Redshift Survey sample, as are the corrections implied at $z \sim 0.3$ in comparison to the results of Tresse & Maddox (1998).

Because the faint ends of luminosity functions have not been well established at high redshifts, and the uncertainties in dust extinction are large at all redshifts, it is probably safest not to read very much into Figure 9. The point is that there is little compelling evidence, in view of the uncertainties involved, for the “peak” in universal star formation density at $z \sim 1 - 2$ that has been assumed by many authors.

5. DISCUSSION

The precise relationships between the star-formation densities estimated with various techniques (e.g. UV continua, $\text{H}\alpha$, sub-millimeter) are ambiguous because of the uncertainties in both relative normalization and in quantitative interpretation (see, e.g., Kennicutt 1998). On the other hand, the consistency of the method we have used to quantify the UV luminosities being produced by star formation at $z \sim 3$ and $z \sim 4$, coupled with more secure knowledge of the relevant volumes being probed because of the extensive spectroscopic sub-samples, allows for a much more robust differential determination than has been possible up to this time. While we still regard our result as tentative because of the relatively small size of the $z \sim 4$ spectroscopic sample, it should serve as a caution against reaching premature conclusions about the extent to which the universal star formation history is understood.

5.1. Differences Between the Current Sample and the HDF

There is not strictly speaking any conflict between the results we have presented and analyses based solely on the Hubble Deep Field (e.g. Madau *et al.* 1996, MPD, etc.). Our ground-based data are consistent with HDF at both $z \sim 3$ and $z \sim 4$ in the range of apparent magnitudes that overlap, although this range is very small at $z \sim 4$. The HDF provides the only data on fainter LBGs at these redshifts. In §4.3 we re-analyzed the HDF using improved estimates of the intrinsic spectral-energy distributions of high-redshift galaxies, and we found, like previous authors, that the co-moving luminosity density of faint LBGs in the HDF appears to be roughly 2 times lower at $z \sim 4$ than $z \sim 3$. This may indicate that the shape of the luminosity function changes significantly between redshifts $z \sim 4$ and $z \sim 3$ —Sawicki *et al.* (1997) reached this conclusion on somewhat different grounds—but the good agreement of the the $z \sim 3$ and $z \sim 4$ luminosity functions at the bright end, where they are the best determined, makes us suspect instead that the luminosity function may have the same shape at fainter magnitudes as well, and that the small number of

B_{450} dropouts is due to sample variance in the HDF. This would not be unexpected given the strong clustering that LBGs are known to exhibit.

Although the clustering strength of faint LBGs at $z \sim 4$ is not likely to be measured in the near future, we can explore this hypothesis further by assuming that the HDF B_{450} -dropouts have the same clustering strength as brighter LBGs at $z \sim 3$. In our ground-based sample at $z \sim 3$, the variance of galaxy counts N about the mean μ in random regions with angular size similar to the HDF is larger than the Poisson variance $\langle(N - \mu)^2\rangle = \mu$ by an amount $\mu^2\sigma_{\text{gal}}^2$ with $\sigma_{\text{gal}} \sim 0.25$. Because projection effects are comparable in the $z \sim 3$ ground-based and $z \sim 4$ HDF samples, a similar value of σ_{gal} would hold for the HDF B_{450} -dropouts if they exhibited the same clustering as LBGs in our $z \sim 3$ ground-based sample. If the $\alpha = -1.6$ luminosity function shown in the bottom panel of Figure 8 were the correct LBG luminosity function at $z \sim 4$, one would expect an HDF-sized field to contain an average of about 23 B_{450} -dropouts with an RMS of 7.5. The observed number of B_{450} -dropouts, 13, is therefore inconsistent with this scenario at only the 1.3σ level. The formal level of inconsistency would be smaller still if we had taken proper account of other uncertainties (e.g. effective volumes, incompleteness corrections, and so on) in this crude calculation. The null hypothesis of identical luminosity function shapes at $z \sim 3$ and $z \sim 4$ cannot be ruled out with much confidence.

The simulations of Ferguson (1998) suggest another reason why the luminosity density inferred from B_{450} -dropouts in the HDF might be misleadingly low. Magnitudes in the HDF are measured above a fixed isophotal level, and surface brightness dimming will cause objects’ luminosities to be underestimated more at higher redshifts. The magnitude of this effect clearly depends on galaxies’ radial profiles. For his model galaxies, Ferguson estimates that luminosity densities derived from HDF Lyman-break galaxies will be too low by a factor of 1.5 at $z \sim 3$ and 4.7 at $z \sim 4$. Ground-based luminosities will be affected far less, since the galaxies are unresolved and isophotes are forced to be large by atmospheric seeing, and so this effect could by itself explain why the ratio of HDF to ground-based LBG number density appears lower at $z \sim 4$ than $z \sim 3$ —though (as we have argued above) the apparent difference in the ratios does not have much statistical significance.

5.2. Implications of a Constant UV Luminosity Density at High Redshift

If the far-UV luminosity function is unchanged between $\langle z \rangle = 4.13$ and $\langle z \rangle = 3.04$, there are some interesting implications. Before discussing these, it is worth mentioning (again) that the *observed* UV luminosity function may be quite different from one which has been corrected for extinction by dust (we are in the process of exploring the possibility of constraining the “true” UV luminosity function at $z \sim 3$ using the large LBG sample). If internal extinction were significantly more important at $z \sim 3$ than at $z \sim 4$, it would still be possible to accommodate a substantial decrease in the star formation activity at higher redshift. However, increasing the extinction tends to have a significant effect on the shape of the LF as well as the normalization (because the level

of extinction appears to be a function of intrinsic luminosity at both low redshift and in the $z \sim 3$ Lyman-break galaxy sample), so that if the dust properties were very different between the two epochs, they would have to conspire to yield very similar observed distributions. Moreover, although our lever arm for measuring the UV spectral energy distributions of the $z \sim 4$ galaxies is not really adequate for independent assessment of their implied “reddening”, the assumption that the distribution of galaxy colors is the same at $z \sim 4$ as observed at $z \sim 3$ has yielded a redshift distribution that is in good agreement with the (admittedly limited) information on $N(z)$ at $z \sim 4$. Measurements at longer wavelengths (e.g., J or possibly even z band) of the $z > 4$ galaxies and a larger spectroscopic sample will make this kind of statement more secure.

If the luminosity density produced by star formation is really flat between $z \sim 3$ and $z \sim 4$, then this would for the first time provide strong evidence for a divergence of the universal behavior of star formation as compared to that of the space density of luminous AGNs. It is a general result for both optically selected (Schmidt *et al.* 1995, Kennefick *et al.* 1995, Warren, Hewett, & Osmer 1994) and radio-selected QSOs (Hook, Shaver, & McMahon 1998; Shaver *et al.* 1998) that the space density of bright QSOs decreases by a factor of $\sim 3 - 4$ between $z \sim 3$ and $z \sim 4$. A similar, or slightly larger, decline is observed in the (radio) luminosity density of the radio galaxy population in the same range of redshifts (Dunlop 1997). Many have remarked in retrospect that it would not be surprising if star formation density and AGN number density followed similar histories, since the formation of galaxies capable of prodigious star formation and those able to develop massive central black holes must be correlated to some extent. On the other hand, in light of the data presented here, it is probably not difficult to come up with reasons why they might not behave in precisely the same way, particularly at the highest redshifts (c.f. Haehnelt and Rees 1993).

Very recently, there have been a number of exciting results of galaxy surveys conducted at wavelengths of $850 \mu\text{m}$ using the the SCUBA bolometer array on the James Clerk Maxwell telescope (e.g., Smail *et al.* 1997, Blain *et al.* 1998, Hughes *et al.* 1998, Barger *et al.* 1998, Lilly *et al.* 1998, Eales *et al.* 1998), inspiring a great deal of speculation on the implications for the star formation history of the universe, particularly at high redshift. While it is not yet clear how much overlap there will be between luminous sub-millimeter sources and Lyman-break galaxies, if there is any correlation with the bright end of the (observed) UV-selected galaxy luminosity function and potential sub-millimeter sources, then it might be expected that the luminosity density of sub-mm (rest-frame far IR) sources will remain high at $z \sim 4$. On the other hand, if the brightest sub-millimeter sources are related primarily to AGN activity rather than star formation (the only published, positive identification of a high redshift sub-mm source indeed has an AGN component—Iverson *et al.* 1998) then one might instead expect a peak in the $z \sim 2 - 3$ range with a substantial decline at higher redshift. A meaningful comparison between the SCUBA results and those presented here is not possible at present because, as we have shown, the luminosity densities require an accurate knowledge of the effective volume of a survey and also the luminosity distribution. Neither is available for the SCUBA sources pending larger spectroscopic samples, no

matter how elaborate a model one constructs.

5.3. Comparison With Expectations of Models of Galaxy Formation

In a comprehensive investigation of the universal star formation history and the implications and constraints provided by cosmic backgrounds at various wavelengths, MPD considered a number of different star formation histories, including one designed to mimic the traditional “monolithic collapse”. In this model, there is no decline in the luminosity density produced by star formation at $z > 1$, so that the star formation history looks similar to the extinction-corrected points in Figure 9. In order to reproduce the observed data for the UV luminosity density in the HDF, it was necessary to add dust extinction whose importance was an increasing function of redshift. Given the new data, as shown above, it is possible to accommodate a similar star formation history without requiring that the role played by dust change in any way as a function of redshift. As pointed out by MPD, because of the limited time involved at the highest redshifts, the only significant impact of having a larger amount of star formation at high redshift is to exceed the mean metallicity as expressed in the chemical abundances of high redshift damped Lyman α systems near $z \sim 3$. However, it may well be that the DLAs do not, and in fact are not expected to, trace the same objects as appear to be producing the bulk of the high redshift stars and metals (Pettini *et al.* 1998b, Somerville, Primack, & Faber 1998, Mo, Mao, & White 1998). Once this constraint is removed, it appears that more high-redshift star formation is not in strong contradiction with any of the observable integrated backgrounds.

An interesting question is whether the observed constant star-formation density between redshifts 3 and 4 is consistent with hierarchical models for structure formation. An upper limit to the star-formation density at a given redshift is the rate at which gas can cool within the virialized objects at that redshift. If the Lyman-break galaxies which we observe are associated with only the most massive virialized dark halos, as we have argued in Adelberger *et al.* (1998), then bremsstrahlung emission will likely be a major component of the cooling rate and supernova feedback will be nearly negligible. In this case, assuming self-similar gas distributions, the hot gas in an observed galaxy would lose energy at a rate $L_{\text{brems}} \propto r_{\text{vir}}^3 \rho^2 T^{1/2}$. The hierarchical scaling relations $r_{\text{vir}}^3 \propto M/(1+z)^3$, $\rho \propto (1+z)^3$, $T^{1/2} \propto v_c \propto M^{1/3}(1+z)^{1/2}$ (e.g. Kaiser 1986, Navarro, Frenk & White 1997) then imply $L_{\text{brems}} \propto M^{4/3}(1+z)^{7/2}$. Approximating the rate at which cold gas is produced, \dot{M}_{cool} , as $L_{\text{brems}} \propto \dot{M}_{\text{cool}} v_c^2$ gives $\dot{M}_{\text{cool}} \propto M^{2/3}(1+z)^{5/2}$. We can estimate the ratio of typical galaxy masses in our $z = 3$ and $z = 4$ samples using the Press-Schechter (1974) model as described (for example) in Adelberger *et al.* (1998). For the $\Gamma \sim 0.2$ power spectrum shape suggested by local measurements, the galaxies in our $z \sim 4$ sample would have typical masses a factor of 3, 1.3, 2 times lower than galaxies of comparable abundance in our $z \sim 3$ sample for $\Omega_M = 1$, $\Omega_M = 0.2$ open, and $\Omega_M = 0.3$ flat. We would therefore expect our samples of galaxies at $z \sim 3$ and $z \sim 4$ to receive newly cooled gas at comparable rates; using the expression above, we estimate that \dot{M}_{cool} is about 1.2, 0.9, 0.7 times higher in $z \sim 3$ sample than our $z \sim 4$

sample—though it would be a mistake to take these numbers too seriously, as our estimate of \dot{M}_{cool} is rather crude. Perhaps a better estimate of the cooling rate is $\dot{M}_{\text{cool}} \propto M^{5/6}(1+z)^2$, proposed (for $\Omega_M = 1$) by White & Frenk (1991), but this would not substantially alter our conclusion that comparable amounts of newly cooled gas are available in our $z \sim 3$ and $z \sim 4$ samples. The point is that two general characteristics of hierarchical models—objects which form at higher redshift are less massive and more dense than objects which form at lower redshift—have opposite effects on the rate at which gas cools in virialized objects, and, over the redshift interval $z \sim 4$ to $z \sim 3$, these opposite effects largely cancel out under a range of plausible assumptions. This suggests that the observed constant star-formation density between $z \sim 4$ and $z \sim 3$ is by no means unexpected in hierarchical models—and indeed it was predicted as early as 1991, long before the relevant observations were made, by White & Frenk (1991, Fig. 5).

A separate question is whether the constant star-formation density is consistent with the prescriptions of semi-analytic models for turning cooled gas into stars. The arguments of the previous paragraph suggest that typical star formation rates in massive halos will need to scale moderately with halo dark mass M and more strongly with redshift z to successfully reproduce the constant star formation density we have observed. Our uncertainty in the evolution of the star formation density from $z \sim 4$ to $z \sim 3$ is still rather large, and we will not press this argument further here; but in principle it will be possible with observations such as these to empirically constrain the relationship between halo dark mass and star formation rate. This largely unconstrained relationship has proven in the past to be a fertile source of free parameters for semi-analytic models; that may not be the case much longer.

The very steep faint end slope ($\alpha = -1.60$) suggested by the current composite $z \sim 3$ LBG luminosity function (Figure 8), if taken at face value, suggests that the majority of the luminosity density at $z \sim 3$ could be produced by objects that are beyond the detection limits for color-selected high redshift galaxies even in Hubble Deep Field data. However, in the context of hierarchical galaxy formation models, if the star formation rates are related to the dark matter halo masses in a monotonic way (cf. Adelberger *et al.* 1998), then at some point the luminosity function is expected to become much less steep than the mass function because of feed-back effects (e.g., Cole *et al.* 1994). For this reason, it would probably be incorrect to assume that the galaxy far-UV luminosity function could remain as steep as observed to arbitrarily faint magnitudes. The implications for galaxy formation models of the far-UV luminosity function and its evolution at high redshift will be explored in much more detail in Adelberger *et al.* 1999. Finally, the faint end slope we derive for the $z \sim 3$ LBG luminosity function is very similar to that determined for far-UV selected galaxies at $z \sim 0.15$, $\alpha = -1.62$ (Treyer *et al.* 1998).

The current uncertainties in the observed UV luminosity function at $z \gtrsim 4$ (and therefore the uncertainties in epoch-to-epoch comparisons) will certainly be reduced as more redshifts are obtained, and it is clearly interesting in light of the discussion above to probe fainter into the $z \sim 4$ luminosity function with wide-angle surveys. More spectroscopy will allow more precise estimates of the effective volume imposed by a given set of color selection criteria, and will allow

a better determination of the range of galaxy properties observed at a given redshift. There is of course the possibility of extending this type of survey to higher redshifts, as shown by recent successes in identifying galaxies at $z > 5$ (Dey *et al.* 1998; Weymann *et al.* 1998; Lanzetta, Yahil, & Fernandez-Soto 1996). The difficulty will come in gathering enough statistics to quantify the galaxy population at extreme redshifts, as one will be forced to still fainter apparent magnitudes (in order to observe the same range of intrinsic luminosities) and longer wavelengths for the follow-up spectroscopy, and the surface densities will begin to be so small that one will not be able to make optimum use of multi-object spectrographs on large telescopes. A concern is that galaxies without strong Lyman α emission at much higher redshifts are likely to be extraordinarily difficult to confirm spectroscopically. On the other hand, systematic searches for much higher redshift galaxies, and follow-up spectroscopy, would be easily within reach with IR cameras and spectrographs on NGST.

6. SUMMARY

We have presented new photometric data covering 828 square arc minutes, and spectroscopic redshifts for 48 of the 244 candidates to $I_{AB} = 25.0$, for Lyman-break galaxies in the redshift range $3.8 \lesssim z \lesssim 4.5$. These objects were selected using criteria that facilitate a direct comparison to the properties of the Lyman-break galaxies in a larger sample covering the range $2.7 \lesssim z \lesssim 3.4$. Besides demonstrating the feasibility of assembling large samples of $z \gtrsim 4$ galaxies with ground-based imaging and spectroscopy, we have reached the following principal conclusions:

1. The spectroscopic properties of LBGs at $z \gtrsim 4$ are very similar to those of the brighter LBGs at $z \sim 3$. There is a wide range of spectroscopic properties, and the Lyman α line appears only in absorption for $\sim 50\%$ of the spectroscopically confirmed objects. We have used the results of the spectroscopy to fine-tune the $z \sim 4$ color selection criteria to minimize contamination by lower redshift interlopers, and to maximize the completeness of the photometrically selected samples.

2. We see no evidence in our ground-based samples for a significant change in either the shape or normalization of the LBG luminosity function between redshifts $\langle z \rangle = 4.13$ and $\langle z \rangle = 3.04$. Of our results, this is the one which depends upon the fewest assumptions. It holds for each of the cosmologies we consider ($\Omega = 1$, $\Omega = 0.2$ open, $\Omega = 0.3$ flat), and is largely independent of our newly estimated incompleteness corrections. If there is any large change in the UV-luminosity density between $z \sim 4$ and $z \sim 3$, it must be due to objects too faint to be included in our ground-based sample. We agree with several previous authors that the HDF provides some evidence that these intrinsically faint LBGs are rarer at $z \sim 4$ than $z \sim 3$, but the evidence is meager—there are only 13 B_{450} dropouts in the HDF—and is drawn from a small and possibly unrepresentative volume of the universe.

3. We have developed a working model of the distribution of LBG colors which, when folded

in with our color selection criteria and the observational uncertainties, successfully reproduces the observed colors as a function of redshift and the observed redshift distributions in the spectroscopic samples. Within the context of this model, the observed far-UV colors imply that a typical LBG suffers about 1.6 mag. of extinction at 1500Å in the rest frame (cf. Pettini *et al.* 1998a), with a range from zero extinction to ~ 5 magnitudes. If we apply an internally consistent extinction correction to the observed luminosity density points, and assume that dust plays an equal role at all redshifts, we find that the emissivity per unit co-moving volume due to star formation remains *essentially flat* for all redshift $z > 1$; hence, it is not clear that the beginning of the epoch of star formation has yet been identified.

4. We have presented a new composite $z \sim 3$ far-UV luminosity function, based on a combination of data from our ground based survey and from a re-analysis of the HDF data based on our improved estimate of the survey effective volumes. The luminosity function at $z \sim 3$ is well fit by a Schechter function with a faint end slope of $\alpha = -1.60 \pm 0.13$, considerably steeper than previous estimates. A similar fit results from using the ground-based sample alone. Such a steep faint end slope allows for the possibility that a large fraction of the luminosity density at high redshift lies beyond even the detection limits in the Hubble Deep Field. The lack of adequate constraints on the behavior of the LBG luminosity functions at faint magnitudes, particularly at $z \gtrsim 4$, are an additional, possibly large, source of uncertainty in estimating the total luminosity density at high redshifts.

5. The similarity of the (observed) $z \sim 4$ and $z \sim 3$ bright-end luminosity functions indicates a significant difference in the evolutionary behavior of universal star formation as compared to the space density of luminous AGNs.

6. The apparent constancy of the UV luminosity function between $z \sim 3$ and $z \sim 4$ has interesting implications for the redshift distribution for the newly discovered population of luminous sub-millimeter sources, and for the star formation prescriptions in semi-analytic models of galaxy formation.

We are grateful to the many people responsible for building and maintaining the W. M. Keck telescopes and the Low Resolution Imaging Spectrograph. We also thank the dedicated staffs of the Palomar, Keck, Cerro Tololo, and La Palma observatories for making these difficult observations possible. Software by J. Cohen, A. Phillips, and P. Shopbell helped in slit-mask design and alignment. CCS acknowledges support from the U.S. National Science Foundation through grant AST 94-57446, and from the David and Lucile Packard Foundation. MG has been supported through grant HF-01071.01-94A from the Space Telescope Science Institute, which is operated by the Association of Universities for Research in Astronomy, Inc. under NASA contract NAS 5-26555.

REFERENCES

- Adelberger, K.L., Steidel, C.C., Giavalisco, M., Dickinson, M., Pettini, M., & Kellogg, M. 1998, *ApJ*, 505, 18
- Adelberger, K.L., et al 1999, in preparation
- Bagla, J.S. 1998, *MNRAS*, 297, 251
- Barger, A.J., Cowie, L.L., Sanders, D.B., Fulton, E., Taniguchi, Y., Sato, Y., Kawara, K., & Okuda, H. 1998, *Nature*, 394, XXX.
- Baugh, C.M., Cole, S., Frenk, C.S., & Lacey, C.G. 1998, *ApJ*, 498, 504
- Blain, A., Smail, I., Ivison, R., & Kneib, J-P. 1998, *MNRAS*, in press (astro-ph/9806062)
- Calzetti, D. 1997, *AJ*, 113, 162
- Cole, S., Aragon-Salamanca, A., Frenk, C.S., Navarro, J. F., & Zepf, S.E. 1994, *MNRAS*, 271, 781
- Coles, P., Lucchin, F., Mattarese, S., & Moscardini, L. 1998, *MNRAS*, in press (astro-ph/9803197)
- Connolly, A.J., Szalay, A.S., Dickinson, M., SubbaRao, M.U., & Brunner, R.J. 1997, *ApJ*, 486, L11
- Dey, A., Spinrad, H., Stern, D., Graham, J.R., & Chaffee, F.H. 1998, *ApJ*, 498, L93
- Dickinson, M. 1998, in *The Hubble Deep Field*, eds. M. Livio, S.M. Fall, & P. Madau 1998, (Cambridge: Cambridge University Press), in press (astro-ph/9802064)
- Dunlop, J. 1997, in *Cosmology with the New Radio Surveys*, eds. M. Bremer et al., (Dordrecht: Kluwer), in press (astro-ph/9704294)
- Eales, S., Lilly, S., Gear, W., Dunne, L., Bond, J.R., Hammer, F., Le Fèvre, O., & Crampton, D. 1998, *ApJ*, submitted (astro-ph/9808040)
- Ferguson, H. C., 1998, in *The Hubble Deep Field*, eds. M. Livio, S. M. Fall, & P. Madau 1998, (Cambridge: Cambridge University Press), in press (astro-ph/9801058)
- Giavalisco, M., Steidel, C. C., Adelberger, K. L., Dickinson, M. E., Pettini, M., & Kellogg, M. 1998a, *ApJ*, 503, 543
- Glazebrook, K. Blake, C., & Economou, F. 1998, *MNRAS*, submitted
- Governato, F., Baugh, C. M., Frenk, C. S., Cole, S., Lacey, C. G., Quinn, T., & Stadel, J. 1998, *Nature*, 392, 359
- Haehnelt, M., & Rees, M. J. 1993, *MNRAS*, 263, 168
- Hook, I.M., Shaver, P.A., & McMahon, R.G. 1998, in *The Young Universe: Galaxy Formation and Evolution at Intermediate and High Redshift*, eds. S. d’Odorico, A. Fontana, & E. Giallongo (San Francisco: ASP), p. 17
- Hu, E.M., Cowie, L.L., & McMahon, R.G. 1998, *ApJ*, 502, L99
- Hughes, D., Serjeant, S., Dunlop, J., Rowan-Robinson, M., Blain, A., Mann, R.G., Ivison, R., Peacock, J., Efstathiou, A., Gear, W., Oliver, S., Lawrence, A., Longair, M., Goldschmidt, P., & Jenness, T. 1998, *Nature*, 394, 241

- Iverson, R., Smail, I., Le Borgne, J-F., Blain, A., Kneib, J-P., Bezecourt, J., Kerr, T.H., & Davies, J.K. 1998, MNRAS, 298, 583
- Jing, Y.P., & Suto, Y. 1998, ApJ, 494, L5
- Kaiser, N. 1986, MNRAS, 222, 323
- Katz, N.S., Hernquist, L., & Weinberg, D.H. 1998, ApJ, submitted (astro-ph/9806257)
- Kennefick, J.D., Djorgovski, S.G., & de Carvalho, R. R. 1995, AJ, 110, 2553
- Kennicutt, R.S. 1998, ARAA, in press (astro-ph/9807187)
- Lanzetta, K.M., Yahil, A., & Fernandez-Soto, A. 1996, Nature, 381, 759
- Lilly, S., Eales, S., Gear, W., Bond, J.R., Dunne, L., Hammer, F., LeFèvre, O., & Crampton, D. 1998, in NGST: Science and Technological Challenges, ESA, in press (astro-ph/9807261)
- Lilly, S.J., LeFèvre, O., Hammer, F., & Crampton, D. 1996, ApJ, 460, L1
- Madau, P. 1995, ApJ, 441, 18
- Madau, P., Pozzetti, L., & Dickinson, M.E. 1998, ApJ, 498, 106 (MPD)
- Madau, P., Ferguson, H.C., Dickinson, M., Giavalisco, M., Steidel, C.C., & Fruchter, A. 1996, MNRAS, 283, 1388
- Mo, H., Mao, S., & White, S.D.M. 1998, MNRAS, submitted (astro-ph/9807341)
- Navarro, J. F., Frenk, C. S., & White, S. D. M. 1997, ApJ, 490, 493
- Oke, J. B. et al. 1995, PASP 107, 3750
- Oke, J.B., & Gunn, J.E. 1983, ApJ, 266, 713
- Pascarelle, S. M., Lanzetta, K. M., & Fernandez-Soto, A. 1999, ApJ, in press (astro-ph/9810060)
- Pettini, M., Kellogg, M., Steidel, C. C., Dickinson, M., Adelberger, K. L., & Giavalisco, M. 1998a, ApJ, in press (astro-ph/9806219)
- Pettini, M., Ellison, S., Steidel, C.C., & Bowen, D.V. 1998b, ApJ, in press (astro-ph/9808017)
- Pozzetti, L., Madau, P., Zamorani, G., Ferguson, H.C., & Bruzual, G.A. 1998, MNRAS, submitted (astro-ph/9803144)
- Press, W.H., & Schechter, P. 1974, ApJ, 187, 425
- Sawicki, M. J., Lin, H., & Yee, H. K. C. 1997, AJ, 113, 1
- Schechter, P. 1976, ApJ, 203, 297
- Schmidt, M., Schneider, D.P., & Gunn, J.E. 1995, AJ, 110, 68
- Shaver, P., Hook, I.M., Jackson, C.A., Wall, J.V., & Kellermann, K.I. 1998, in Highly Redshifted Radio Lines, eds. C. Carilli, S. Radford, K Menten, & G. Langston (astro-ph/9801211)
- Smail, I., Blain, A., Iverson, R. 1997, ApJ, 490, L5
- Somerville, R.S., Primack, J.R., & Faber, S.M. 1998, MNRAS, submitted (astro-ph/9806228)

- Steidel, C.C., Adelberger, K. L., Dickinson, M., Giavalisco, M., Pettini, M. & Kellogg, M. 1998a, ApJ, 492, 428
- Steidel, C.C., Adelberger, K. L., Giavalisco, M., Dickinson, M., Pettini, M. & Kellogg, M. 1998b, Phil.Trans. R.S., in press (astro-ph/9805267).
- Steidel, C.C., Giavalisco, M., Pettini, M., Dickinson, M., & Adelberger, K. L. 1996a, ApJ, 462, L17
- Steidel, C.C., Giavalisco, M., Dickinson, M., & Adelberger, K.L. 1996b, AJ, 112, 352.
- Steidel, C.C., Pettini, M., & Hamilton, D. 1995, AJ, 110, 2519
- Steidel, C.C., & Hamilton, D. 1993, AJ, 105, 2017
- Tresse, L., & Maddox, S.J. 1998, ApJ, 495, 691
- Treyer, M. A., Ellis, R.S., Milliard, B., Donas, J., & Bridges, T.J. 1998, MNRAS, in press (astro-ph/9806056)
- Valdes, F. 1982, FOCAS User's Manual (NOAO, Tucson)
- Warren, S.J., Hewett, P.C., & Osmer, P.S. 1994, ApJ, 421, 412
- Wechsler, R. H., Gross, M. A. K., Primack, J. R., Blumenthal, G. R. & Dekel, A. 1998, ApJ, submitted (astro-ph/9712141)
- Weymann, R.J., Stern, D., Bunker, A., Spinrad, H., Chaffee, F.H., Thompson, R.I., & Storrie-Lombardi, L.J. 1998, ApJ, submitted (astro-ph/9807208)
- White, S.D.M., and Frenk, C.S. 1991, ApJ, 379, 25

Table 1. $z \gtrsim 4$ Lyman-Break Galaxy Fields

Field Name	Field Center (J2000)	Area (arc min) ²	# Candidates ^a	z_{true} ^b	z_{false} ^c
CDFa	00 53 23.7 +12 34 00	78	22/21	6/5	0/0
CDFb	00 53 43.0 +12 25 15	82	26/22	8/8	1/0
B2 0902+34	09 05 30.2 +34 07 55	40	13/8	3/3	4/1
HDF	12 36 52.3 +62 12 59	75	26/20	2/2	1/0
3C324	15 49 49.6 +21 29 07	42	15/10	2/2	4/2
DSF1550	15 51 02.4 +07 22 34	180	61/58	7/7	1/1
SSA22a	22 17 34.2 +00 15 01	78	28/24	5/5	9/4
SSA22b	22 17 34.2 +00 06 18	78	13/11	3/3	1/0
DSF2237a	22 40 08.5 +11 52 34	83	25/21	6/6	1/1
DSF2237b	22 39 34.3 +11 51 44	82	16/12	6/5	2/1
TOTAL		828	244/207	48/46	25/12

^aThe first entry applies to the initial, broad color selection window; the second entry is the number of candidates remaining after applying the $\mathcal{R} - I \leq 0.6$ color criterion and the $I \geq 23.0$ apparent magnitude cut (see text).

^bNumber of spectroscopic redshifts of $z \sim 4$ galaxies, before and after application of the additional color and magnitude criteria.

^cNumber of spectroscopic redshifts of interloper galaxies ($z \ll 4$, before and after application of additional color and magnitude criteria).

Table 2. Lyman-Break Galaxy Candidate Spectroscopic Results

Object Name	RA (J2000)	Dec (J2000)	I_{AB}	$(\mathcal{R} - I)_{AB}$	$(G - \mathcal{R})_{AB}$	z
CDFa-G1	00 53 33.25	+12 32 07.3	23.59	0.89	>3.72	4.815
CDFa-GD3	00 53 26.93	+12 30 45.6	24.92	-0.18	2.47	4.050
CDFa-GD4	00 53 36.20	+12 31 09.1	23.49	0.28	2.07	4.189
CDFa-GD7	00 53 35.60	+12 31 44.2	23.55	0.50	3.71	4.605
CDFa-GD9	00 53 36.13	+12 32 50.2	24.80	0.18	2.45	3.864
CDFa-GD14	00 53 24.66	+12 35 31.3	24.74	0.09	2.02	3.613
CDFb-G1	00 53 35.69	+12 21 06.2	24.85	-0.17	>3.24	4.077
CDFb-G5	00 53 51.26	+12 24 21.3	24.84	0.38	>2.77	4.486
CDFb-GD3	00 53 45.68	+12 21 27.3	24.39	0.11	2.06	3.694
CDFb-GD9	00 53 44.41	+12 21 56.8	23.80	0.31	2.17	3.777
CDFb-GD10	00 53 50.58	+12 23 39.7	24.20	0.25	2.75	4.070
CDFb-GD12	00 53 40.69	+12 24 29.3	24.92	0.24	2.32	3.469
CDFb-GD13	00 53 46.59	+12 24 38.4	24.71	0.07	2.11	3.761
CDFb-GD14	00 53 36.49	+12 24 34.2	24.50	0.27	2.35	4.253
B20902-G1	09 05 22.10	+34 07 51.0	24.64	-0.01	>3.13	4.318
B20902-GD5	09 05 18.93	+34 07 51.8	24.67	-0.31	2.68	4.039
B20902-GD11	09 05 34.54	+34 10 26.0	24.23	-0.23	3.44	4.204
HDF-G4	12 37 20.56	+62 11 06.5	24.32	-0.04	>3.70	4.421
HDF-GD4	12 37 10.65	+62 09 35.8	24.99	0.06	2.76	4.129
3C324-G2	15 49 48.65	+21 26 49.8	24.61	0.39	>2.63	4.434
3C324-GD2	15 49 41.12	+21 27 34.5	24.63	0.45	2.58	4.071
DSF1550-G4	15 50 36.23	+07 16 54.6	24.54	0.44	>3.13	4.133
DSF1550-GD10	15 50 56.77	+07 15 42.1	24.83	-0.47	2.25	3.914
DSF1550-GD18	15 50 39.41	+07 16 44.5	24.75	-0.27	2.22	4.144
DSF1550-GD22	15 50 37.14	+07 17 52.8	24.40	-0.17	2.10	3.894
DSF1550-GD23	15 50 44.13	+07 18 20.1	23.97	0.15	2.33	4.053
DSF1550-GD30	15 50 48.31	+07 20 45.5	24.50	0.16	2.30	4.299
DSF1550-GD32	15 50 45.48	+07 20 54.3	24.46	-0.21	2.34	4.176
SSA22a-G3	22 17 30.79	+00 12 50.9	24.65	0.38	>2.83	4.527
SSA22a-G6	22 17 48.39	+00 14 34.5	24.72	-0.06	>3.02	3.710
SSA22a-G11	22 17 39.43	+00 17 46.0	24.91	0.58	2.80	4.390
SSA22a-GD11	22 17 42.78	+00 16 18.1	24.59	0.11	2.23	4.397
SSA22a-GD12	22 17 48.39	+00 16 25.9	24.24	0.17	2.18	4.114
SSA22b-GD7	22 17 32.40	+00 05 32.5	24.47	0.56	2.95	3.895
SSA22b-GD9	22 17 42.49	+00 07 26.4	23.81	0.16	2.14	3.856
SSA22b-GD10	22 17 33.80	+00 08 48.3	23.36	0.40	2.70	4.086
DSF2237a-G3	22 40 03.64	+11 49 12.6	24.75	-0.08	>3.13	4.400
DSF2237a-G7	22 40 13.09	+11 53 32.2	24.70	0.13	>3.28	3.838
DSF2237a-G10	22 40 18.80	+11 55 44.4	24.44	0.52	>3.27	4.467
DSF2237a-GD3	22 40 06.88	+11 49 17.8	24.70	0.14	2.11	3.964
DSF2237a-GD7	22 40 04.34	+11 52 34.7	24.71	-0.15	2.91	4.453
DSF2237a-GD10	22 40 03.87	+11 53 57.5	24.89	-0.02	2.17	4.189
DSF2237b-G2	22 39 39.11	+11 49 20.5	24.33	0.72	>3.35	4.178
DSF2237b-G4	22 39 25.52	+11 50 39.2	24.23	0.38	>3.74	4.492
DSF2237b-G12	22 39 33.25	+11 55 24.9	24.98	0.11	>3.15	4.375
DSF2237b-GD6	22 39 33.52	+11 51 54.6	24.98	-0.06	2.03	4.486
DSF2237b-GD11	22 39 29.09	+11 55 47.0	24.81	0.40	2.97	3.679
DSF2237b-GD12	22 39 30.35	+11 55 54.5	24.28	0.19	2.24	3.868
CDFb-GD4	00 53 30.10	+12 21 24.1	22.72	0.98	4.01	0.000
B20902-GD2	09 05 37.62	+34 05 20.3	23.98	0.57	2.94	1.069
B20902-GD3	09 05 25.20	+34 06 11.1	22.72	0.96	3.47	0.842

Table 2—Continued

Object Name	RA (J2000)	Dec (J2000)	I_{AB}	$(\mathcal{R} - I)_{AB}$	$(G - \mathcal{R})_{AB}$	z
B20902-GD7	09 05 29.88	+34 09 22.0	22.42	0.89	3.59	0.651
B20902-GD8	09 05 30.96	+34 09 31.7	23.75	0.70	3.13	0.944
HDF-GD5	12 37 24.71	+62 09 46.9	22.96	0.58	3.20	1.010
3C324-G1	15 49 50.07	+21 26 23.1	24.35	0.78	>3.12	0.945
3C324-G6	15 49 46.57	+21 29 38.0	24.57	0.51	>2.86	0.941
3C324-G8	15 49 57.19	+21 30 12.8	24.72	0.56	>2.84	0.964
3C324-GD5	15 49 56.95	+21 31 00.2	22.85	0.97	3.54	0.809
DSF1550-GD28	15 50 50.36	+07 20 16.0	23.25	0.27	2.05	0.961
SSA22a-G1	22 17 44.68	+00 12 05.6	23.97	0.75	>3.09	1.061
SSA22a-G4	22 17 23.38	+00 13 14.4	23.85	0.72	>3.09	1.243
SSA22a-G8	22 17 28.77	+00 15 49.2	24.31	0.11	3.11	1.152
SSA22a-GD5	22 17 42.29	+00 13 23.6	23.76	0.58	3.06	0.630
SSA22a-GD7	22 17 33.89	+00 14 50.8	24.17	0.64	2.89	1.109
SSA22a-GD8	22 17 50.49	+00 15 18.2	23.49	0.23	2.14	0.339
SSA22a-GD13	22 17 41.93	+00 16 44.0	24.18	0.24	2.19	0.670
SSA22a-GD14	22 17 29.16	+00 17 11.9	24.78	0.18	2.55	0.740
SSA22a-GD15	22 17 36.56	+00 17 46.8	24.86	0.22	2.04	1.238
SSA22a-GD17	22 17 37.62	+00 18 51.3	22.02	0.90	3.33	0.785
SSA22b-G3	22 17 42.57	+00 02 51.6	23.44	0.82	>3.53	1.0
DSF2237a-GD6	22 40 06.05	+11 50 47.0	23.28	0.52	2.66	0.861
DSF2237b-GD1	22 39 32.24	+11 47 38.0	24.76	0.37	2.87	1.0
DSF2237b-GD3	22 39 26.10	+11 50 19.0	21.15	0.22	2.04	0.499

Table 3. Lyman-Break Galaxy Surface Density and Effective Survey Volumes, $z \sim 3^a$

AB Mag Range ^b	$\Sigma(z = 3)^c$	$V_{\text{eff}}(1, 0)^d$	$V_{\text{eff}}(0.2, 0)^d$	$V_{\text{eff}}(0.3, 0.7)^d$
22.5-23.0	0.002 ± 0.001	120	448	471
23.0-23.5	0.021 ± 0.004	120	448	471
23.5-24.0	0.087 ± 0.011	117	437	459
24.0-24.5	0.194 ± 0.016	112	418	440
24.5-25.0	0.380 ± 0.023	97	362	381
25.0-25.5	0.495 ± 0.049	67	250	263

^aObserved surface density

^b \mathcal{R} magnitudes

^cObjects per arc min² in 0.5 magnitude interval for $z \sim 3$ sample. Each bin has been corrected for contamination by interlopers based on the spectroscopic sample. The errors reflect both Poisson counting and field-to-field variations

^dEffective survey volume per square arc minute for galaxies in each range of apparent magnitude, in units of $h^{-3} \text{ Mpc}^3$. The numbers in parentheses indicate the assumed cosmology, with $(\Omega_m, \Omega_\Lambda)$.

Table 4. Lyman-Break Galaxy Surface Density and Effective Survey Volumes, $z \sim 4^a$

AB Mag Range ^b	$\Sigma(z = 4)^c$	$V_{\text{eff}}(1, 0)^d$	$V_{\text{eff}}(0.2, 0)^d$	$V_{\text{eff}}(0.3, 0.7)^d$
23.0-23.5	0.004 ± 0.002	129	619	537
23.5-24.0	0.014 ± 0.006	129	619	537
24.0-24.5	0.063 ± 0.013	118	566	491
24.5-25.0	0.131 ± 0.015	74	355	308

^aObserved surface density

^b I magnitudes

^cObjects per arc min² in 0.5 magnitude interval for $z \sim 4$ sample. Each bin has been corrected for contamination by interlopers based on the spectroscopic sample. The errors reflect both Poisson counting and field-to-field variations

^dEffective survey volume per square arc minute, in units of h^{-3} Mpc³. The numbers in parentheses indicate the assumed cosmology, with $(\Omega_m, \Omega_\Lambda)$.

Table 5. Observed Ultraviolet Luminosity Densities

Cosmological Model	$\log \rho_{UV}(z = 3)^a$	$\log \rho_{UV}(z = 4)^a$	$\rho_{UV}(z = 3)/\rho_{UV}(z = 4)$
$\Omega_m = 1.0, \Omega_\Lambda = 0$	26.05 ± 0.07	25.96 ± 0.10	1.23 ± 0.38
$\Omega_m = 0.2, \Omega_\Lambda = 0$	25.74 ± 0.07	25.74 ± 0.10	1.02 ± 0.31
$\Omega_m = 0.3, \Omega_\Lambda = 0.7$	25.75 ± 0.07	25.70 ± 0.10	1.13 ± 0.35

^aUV luminosity density in units of $\log(\text{ergs s}^{-1} H z^{-1} h \text{ Mpc}^{-3})$. These numbers are integrated only over the range of luminosities in common to the two ground-based samples; no extrapolation to fainter magnitudes using HDF data or an assumed luminosity function has been included here.

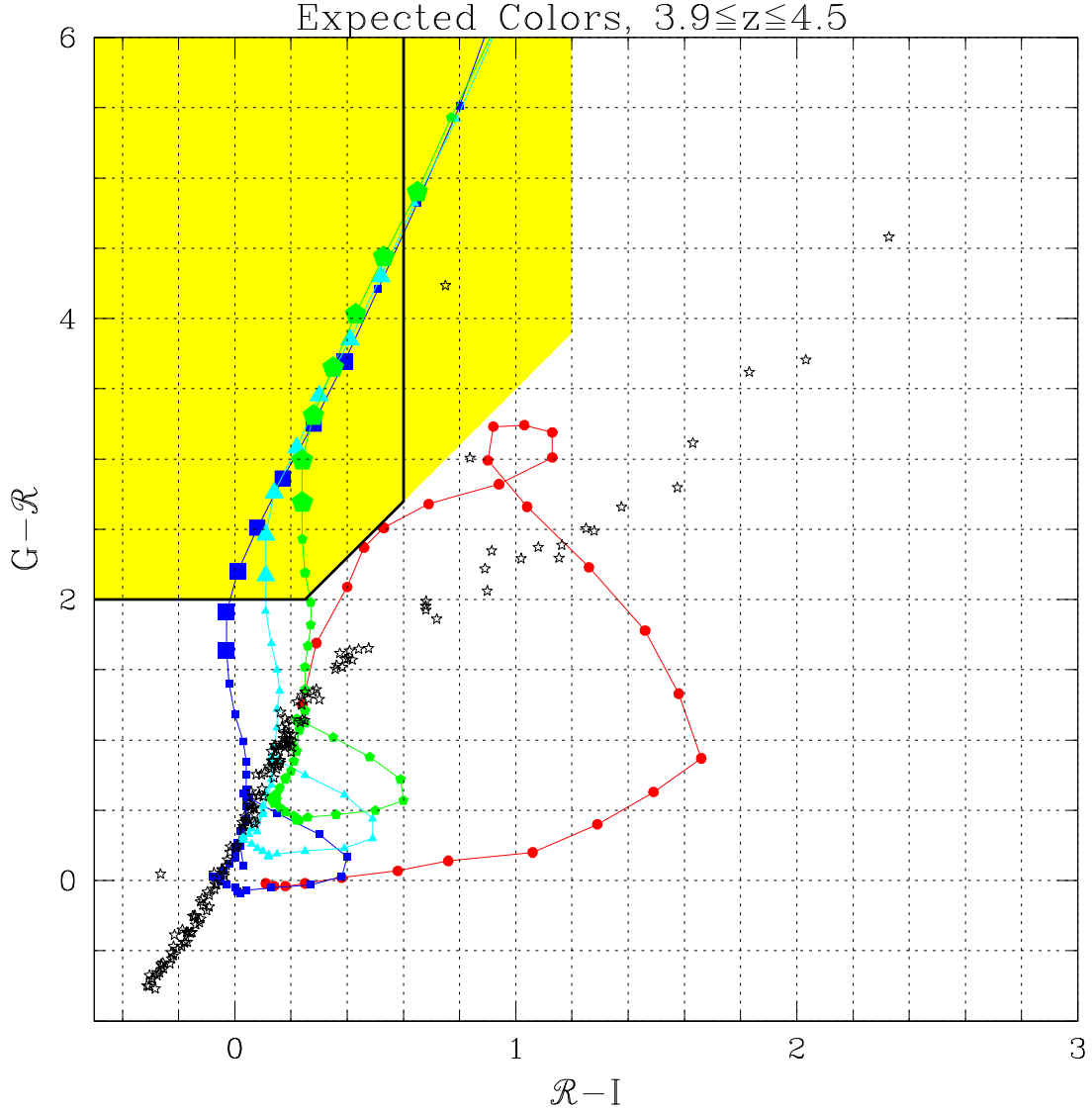


Fig. 1a.— Expected locus of colors versus redshift in the adopted 3-band photometric system, for the $z \sim 4$ sample. The shaded region indicates that used for our initial spectroscopic sample, while the region enclosed with the bold lines is that used for the statistical samples (see text for discussion). The positions in the color-color diagrams expected for 3 different degrees of reddening ($E(B-V)=0, 0.15$, and 0.30) are shown with squares, triangles, and pentagons, respectively. Redshifts in the range $3.9 - 4.5$ are indicated with enlarged symbols. Also shown (solid dots) is the locus for unevolved early type galaxies, ranging from $z=0.1$ to $z=2.5$ in steps of 0.1 . Note that early type galaxies encroach on our selection window for $z \sim 0.5 - 1$. The “star” symbols represent the colors for Galactic stars.

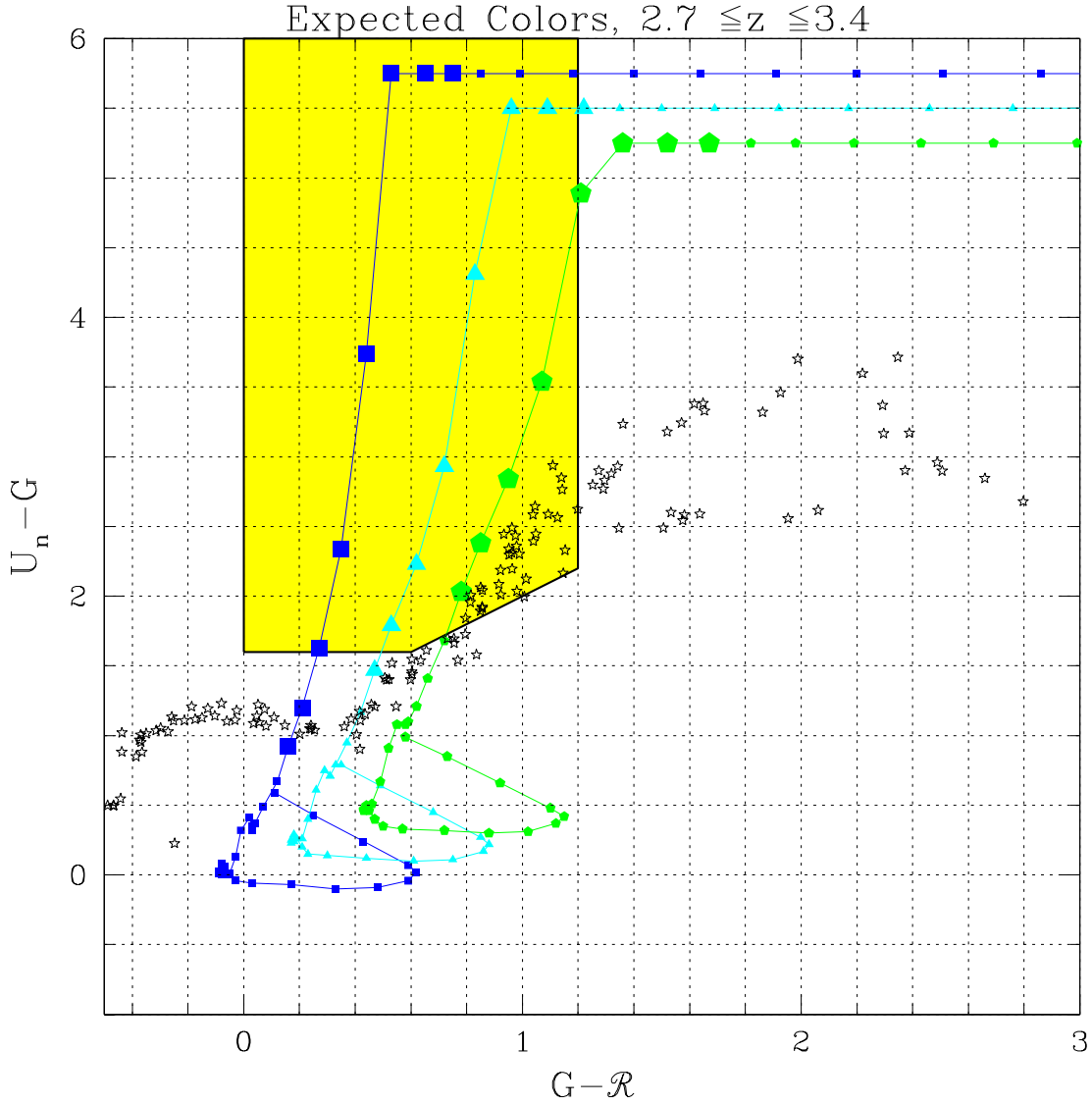


Fig. 1b.— Same as a), for the $z \sim 3$ Lyman-break galaxy selection criteria. Models for which it is predicted that $U_n - G > 6.0$ are shown with the color “clipped” at a constant $U_n - G$ in order to display the expected $G - \mathcal{R}$ colors on the plot. Redshifts from 2.7 to 3.4 are indicated with the enlarged symbols, where again the squares correspond to an unreddened model SED, the triangles to one having $E(B - V) = 0.15$ with the Calzetti reddening law, and the pentagons to one having $E(B - V) = 0.30$. Note that for an object having the “typical” colors (triangles), the selection window is expected to include objects in the full range $2.7 \leq z \leq 3.4$, whereas for the unreddened models one expects only objects toward the higher redshift end of the range, and for the $E(B - V) = 0.3$ tracks, one sees preferentially the lower redshift end of the range.

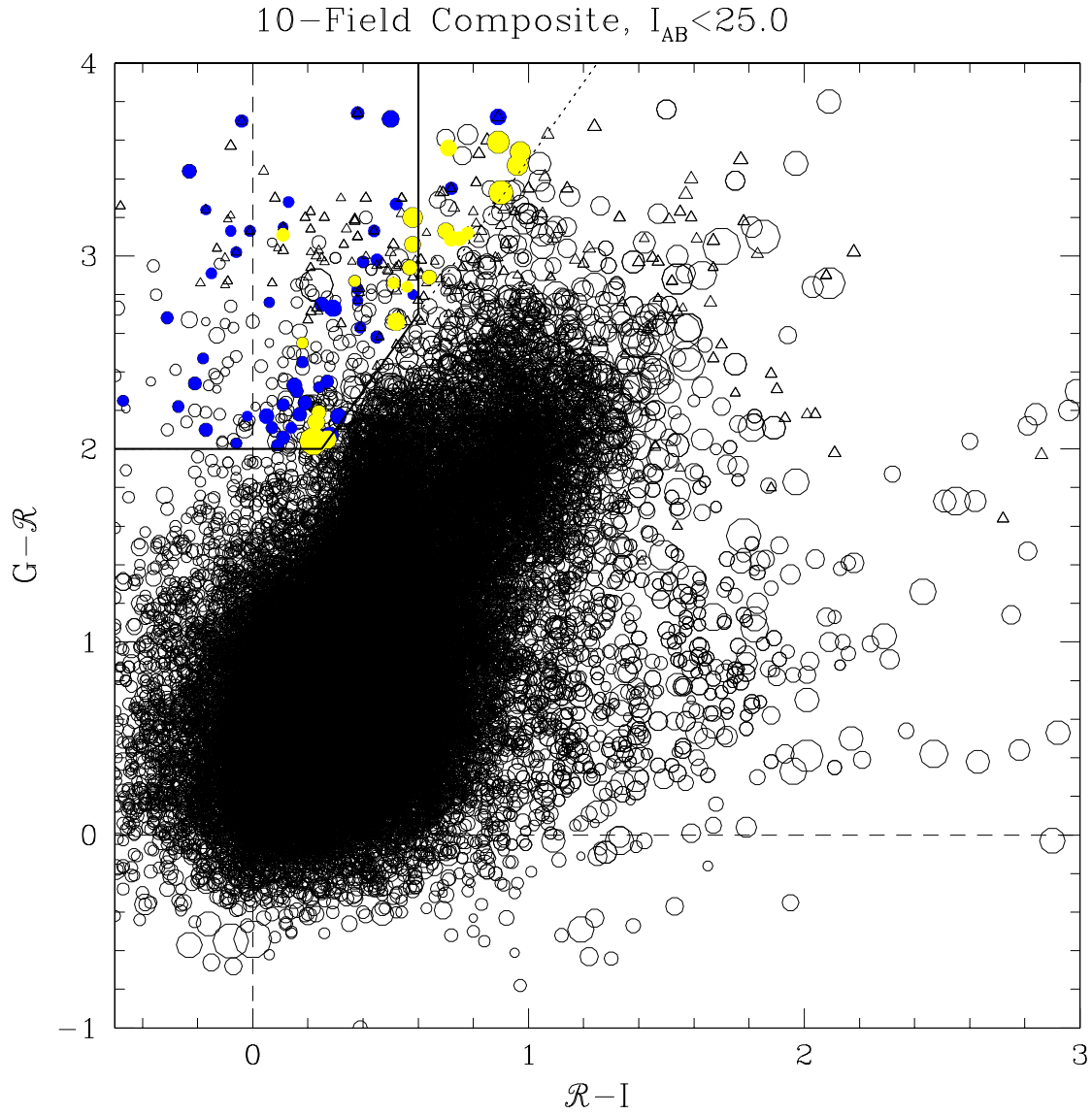


Fig. 2.— 10-Field composite color-color diagram, where the spectroscopic G-band break object selection region is shown enclosed with a dotted line style, and the region used for the statistical samples is indicated with the heavy line type. There are approximately 29,000 objects represented here, of which 207 satisfy the primary color selection criteria. Symbol size scales inversely with apparent magnitude, and triangles represent objects with only limits on the $G - \mathcal{R}$ color. Filled symbols show objects with spectroscopic redshifts, where lighter shading indicates “interloper” galaxies, and darker shading indicates objects with spectroscopic redshifts in the range $3.7 < z < 4.8$.

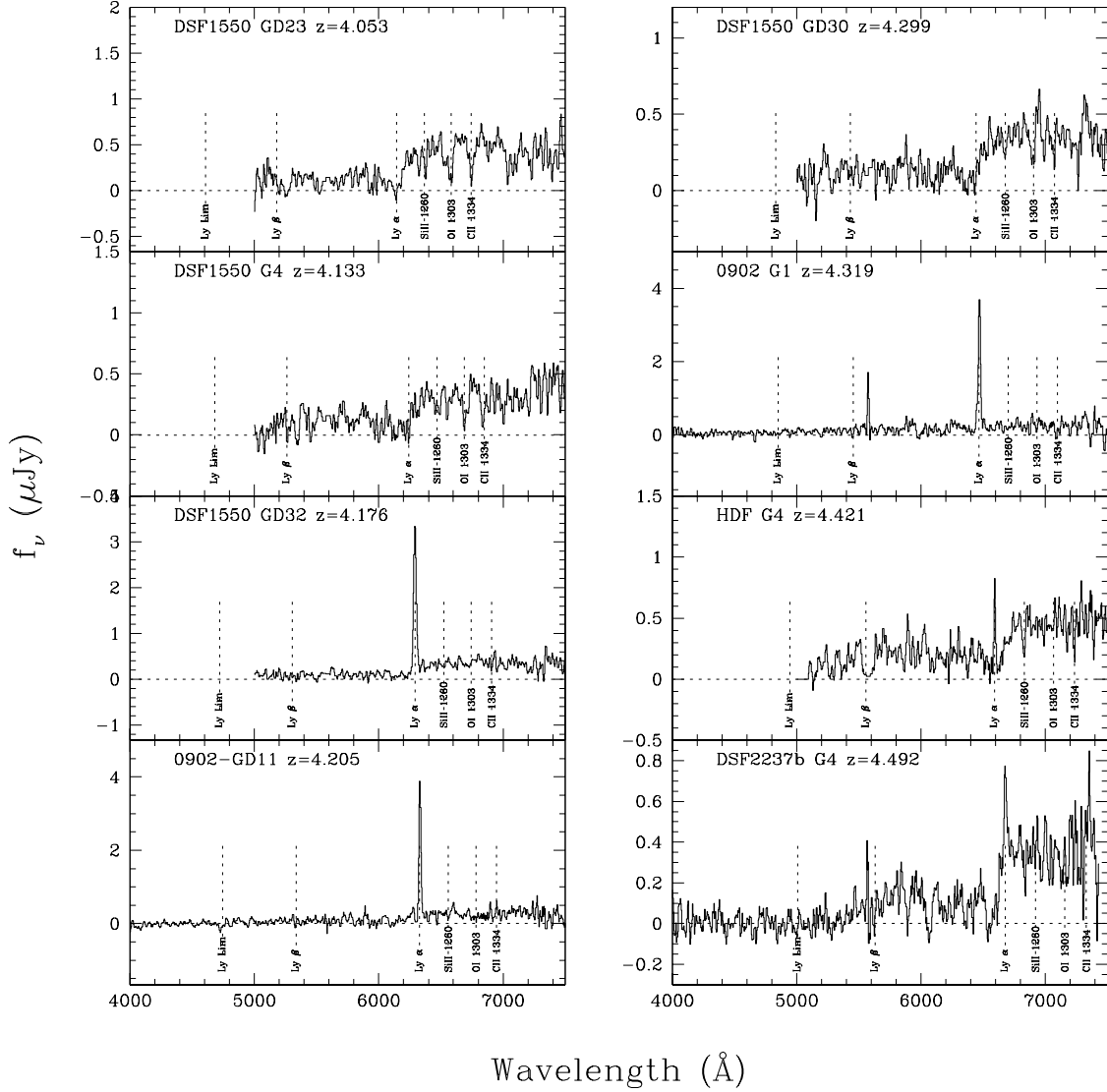


Fig. 3.— Example spectra of G-band break objects. Note that, as for the $z \sim 3$ sample, the $z \sim 4$ Lyman-break galaxies have a widely varying Lyman α line strength, from strong emission lines, to very strong and broad absorption. Overall, the spectra are very similar to the $z \sim 3$ objects at correspondingly bright UV luminosities.

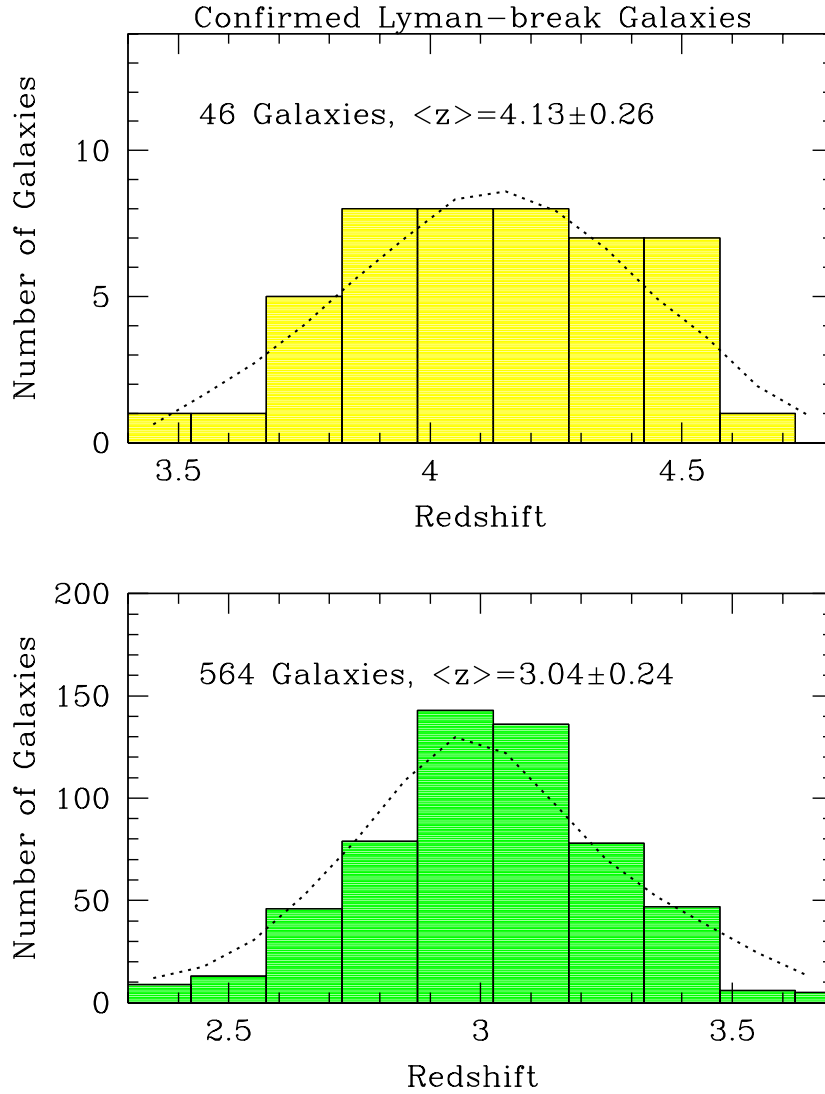


Fig. 4.— Current histogram of $z \sim 4$ Lyman-break galaxies with spectroscopic redshifts (upper panel) and $z \sim 3$ LBGs (lower panel). The mean and standard deviations of the distributions are indicated. The dotted curves are the predicted redshift distributions for our working model (see text) that simultaneously reproduces the observed color distribution as a function of redshift. The curve in the top panel assumes that the intrinsic color distribution of LBGs is the same in the $z \sim 4$ sample as measured in the much-larger $z \sim 3$ sample. .

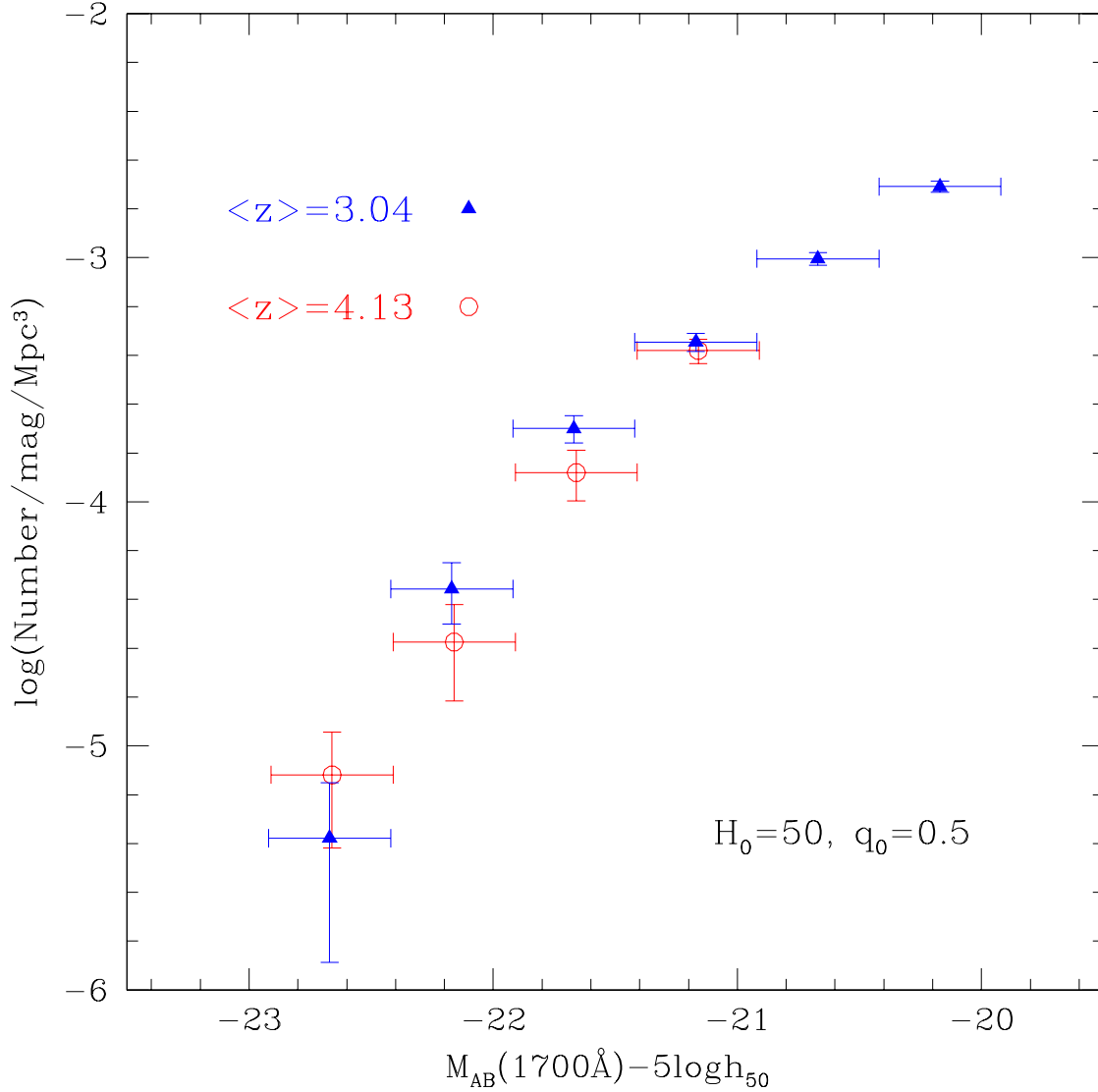


Fig. 5.— A comparison of the luminosity functions for the two Lyman-break galaxy samples, using the effective sample volumes in Tables 3 and 4, and assuming $\Omega = 1$ and $H_0 = 50 \text{ km s}^{-1}\text{Mpc}^{-1}$; other cosmologies considered would result in a shift of the $z \sim 4$ luminosity function to slightly brighter magnitudes relative to $z \sim 3$ (see Table 5 for the effect on the relative luminosity densities).

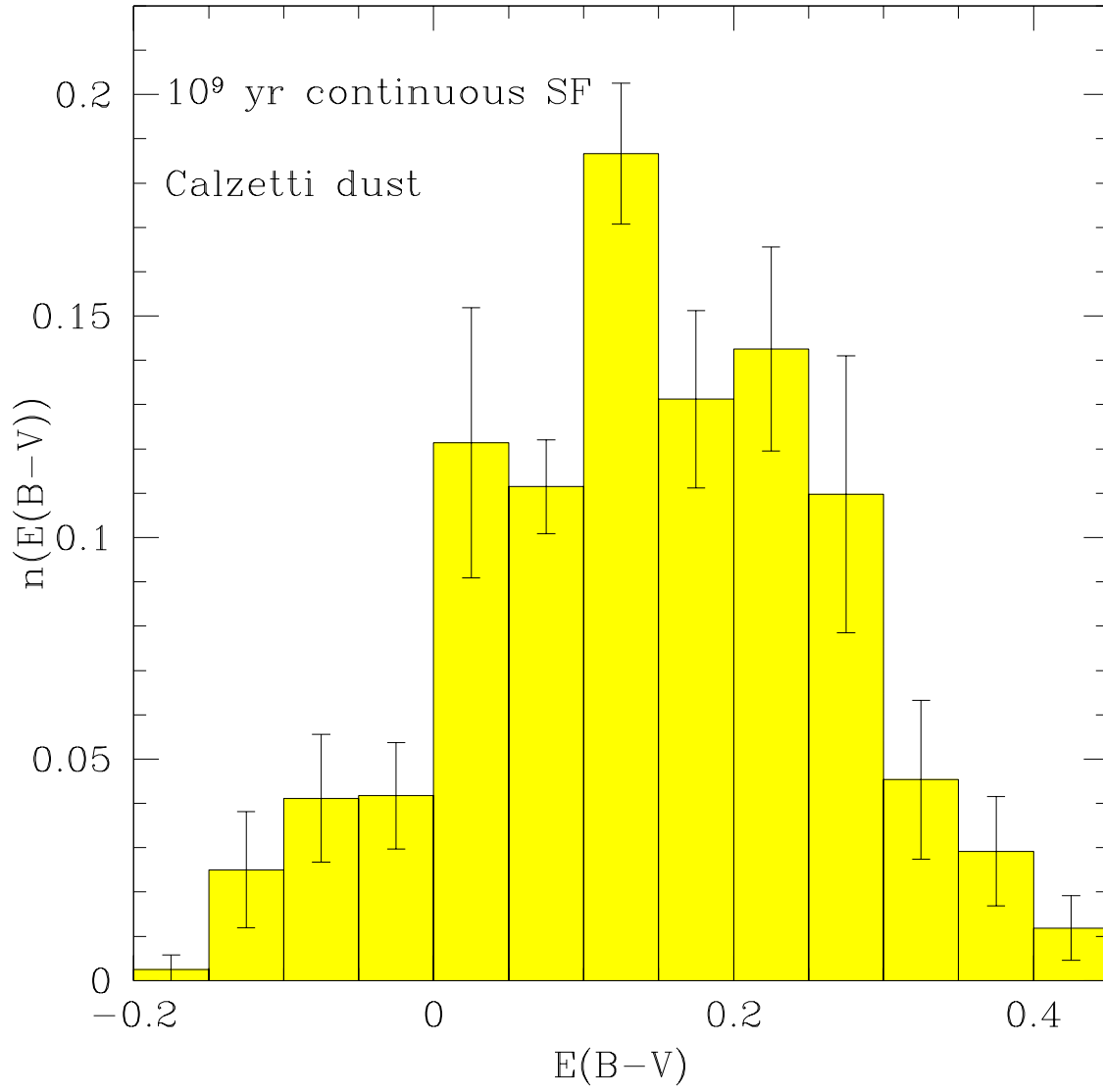


Fig. 6.— The inferred intrinsic distribution of galaxy colors for LBGs at $z \sim 3$. The error bars reflect the field-to-field differences in the color distribution

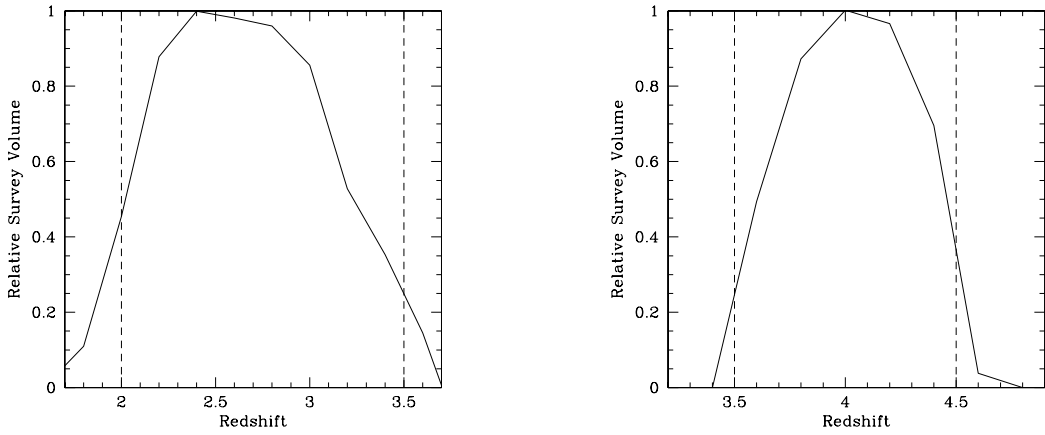


Fig. 7.— Plots showing the expected effective redshift distribution for LBG samples chosen using the HDF filter system and the selection criteria given in the text (cf. Madau *et al.* 1996), if the true density of galaxies remained constant over the redshift interval and if galaxies had the distribution of colors that is found in the ground-based spectroscopic sample. The left panel is for F300W “dropouts”, and the right panel is for F450W “dropouts”. The dashed lines indicate the redshift selection functions assumed by Madau *et al.* (1996, 1998).

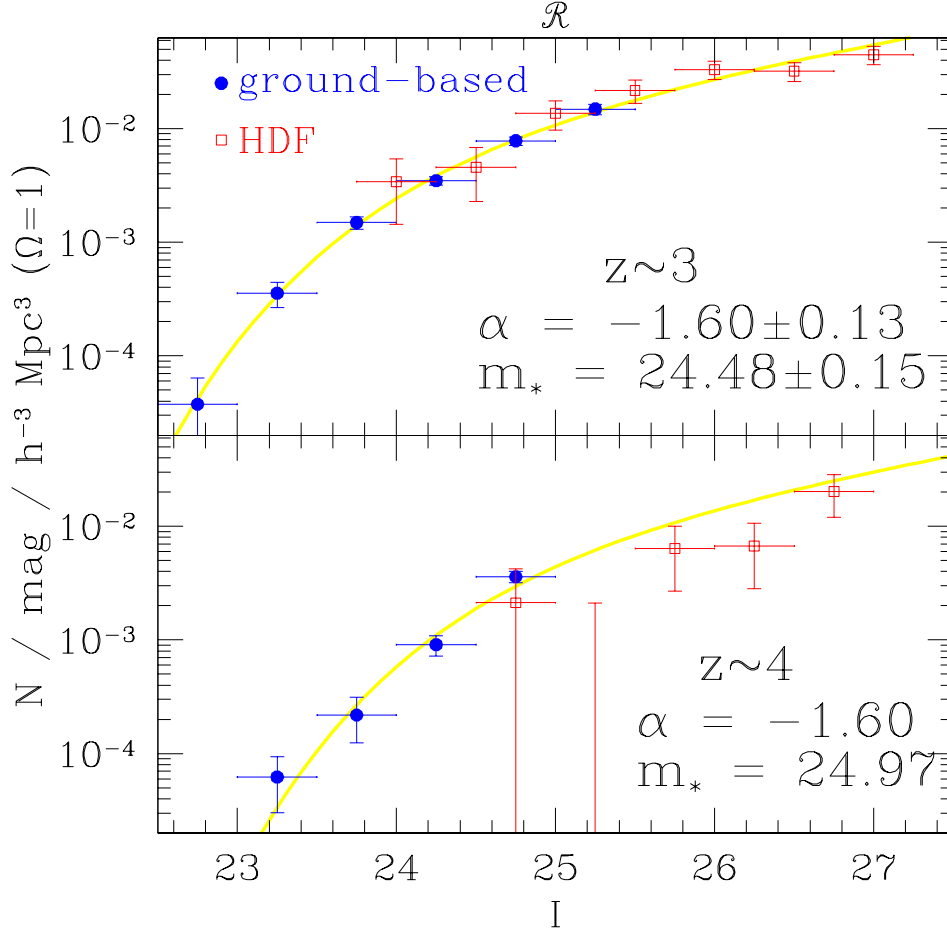


Fig. 8.— Composite ground-based and HDF luminosity distributions for $z \sim 3$ (top) and $z \sim 4$ (bottom). The HDF points account for our new assessment of effective survey volumes. The results of a Schechter (1976) function fit to the $z \sim 3$ luminosity distribution is shown in the top panel. In the bottom panel, the curve shown is the $z \sim 3$ luminosity function shifted by 0.49 magnitudes (the relative distance modulus between $z = 3.04$ and $z = 4.14$ for an Einstein-de Sitter model) with the normalization adjusted to 80% of the $z \sim 3$ value (cf. Table 5, Figure 5). The error bars for the HDF-based points in both panels implicitly assume no clustering of the LBGs (whereas the ground-based points do include this effect) and the “true” error bars are probably significantly larger.

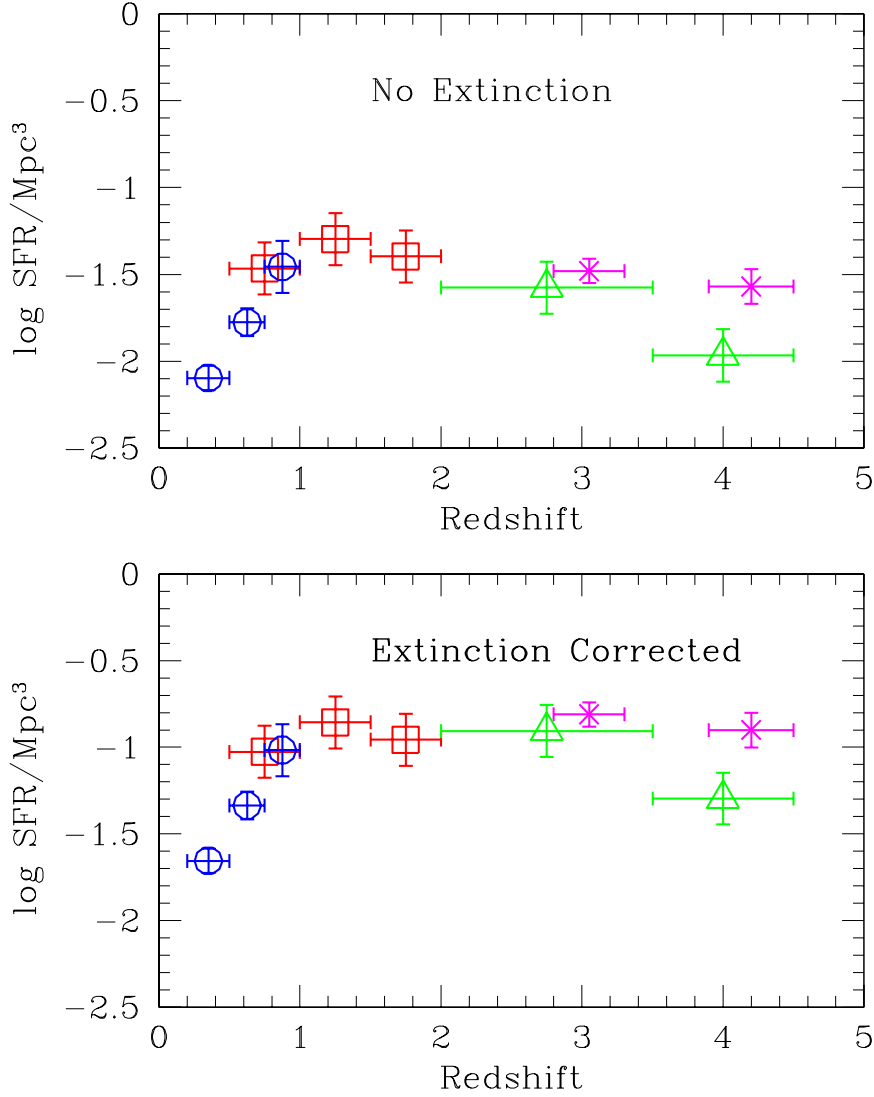


Fig. 9.— The UV luminosity density as a function of redshift, following Madau *et al.* 1996 (also using $H_0 = 50 \text{ km s}^{-1}\text{Mpc}^{-1}$ and $q_0 = 0.5$, for consistency). The different points come from Lilly *et al.* (1996) [circles], Connolly *et al.* (1997) [squares], and Madau *et al.* 1997 (triangles). The new points from this work are shown as crosses. See text for details.)